NAVAL POSTGRADUATE SCHOOL
Monterey, California

THESIS

NATURAL CONVECTION FROM AN ARRAY OF RECTANGULAR PROTRUSIONS IN AN ENCLOSURE FILLED WITH DIELECTRIC FLUID: EFFECTS OF BOUNDARY CONDITIONS, FLUID PRANDTL NUMBER, AND SELECTIVE POWERING.

by

Mark E. Powell

September 1989

Thesis Advisor: Yogendra Joshi

REPORT DOCUMENTATION PAGE

1a REPORT SECURITY CLASSIFICATION: Unclassified	1b RESTRICTIVE MARKINGS
2a SECURITY CLASSIFICATION AUTHORITY	3 DISTRIBUTION/AVAILABILITY OF REPORT: Approved for public release; Distribution is unlimited
2b DECLASSIFICATION/DOWNGRADING SCHEDULE	
4 PERFORMING ORGANIZATION REPORT NUMBER(S)	5 MONITORING ORGANIZATION REPORT NUMBER(S)
6a NAME OF PERFORMING ORGANIZATION: Naval Postgraduate School; 6b OFFICE SYMBOL (If applicable)	7a NAME OF MONITORING ORGANIZATION: Naval Postgraduate School
6c ADDRESS (City, State, and ZIP Code): Monterey CA 93943-5000	7b ADDRESS (City, State, and ZIP Code): Monterey CA 93943-5000
8a NAME OF FUNDING/SPONSORING ORGANIZATION; 8b OFFICE SYMBOL (If applicable)	9 PROCUREMENT INSTRUMENT IDENTIFICATION NUMBER
8c ADDRESS (City, State, and ZIP Code)	10 SOURCE OF FUNDING NUMBERS: PROGRAM ELEMENT NO; PROJECT NO; TASK NO; WORK UNIT ACCESSION NO

11 TITLE (Include Security Classification) Natural Convection from an Array of Rectangular Protrusions in an Enclosure Filled with Dielectric Fluid; Effects of Boundary Conditions, Fluid Prandtl Number, and Selective Powering.

12 PERSONAL AUTHOR(S) Mark E. Powell

13a TYPE OF REPORT	13b TIME COVERED FROM ___ TO ___	14 DATE OF REPORT (Year Month Day)	15 PAGE COUNT
Master s Thesis		September 1989	100

16 SUPPLEMENTARY NOTATION

17 COSATI CODES: FIELD	GROUP	SUB GROUP

18 SUBJECT TERMS (Continue on reverse if necessary and identify by block number) Direct Immersion, Natural Convection Cooling, Dielectric Liquid Protrusions, Enclosure, Simulated Circuit Board, Convective Heat Transfer

19 ABSTRACT (Continue on reverse if necessary and identify by block number)

An experimental investigation has been conducted to further examine Natural Convection Immersion Cooling of a three by three array of heated protrusions in a rectangular chamber filled with dielectric fluid.Each rectangular protrusion geometrically modelled a 20 pin dual inline package.Input power to each component varied from 0.1 to 3.0 W..

The purpose of this study was to examine the effects of the following parameters for the range of power levels selected:1)Top and bottom boundary temperatures;2)Selective powering of components;3)Changes in the Fluid Prandtl number.

The data were obtained as component surface temperatures. These were subsequently presented in terms of appropriate non-dimensional parameters. As part of the overall investigation, flow visualization results are also presented for selected conditions.

20 DISTRIBUTION/AVAILABILITY OF ABSTRACT	21 ABSTRACT SECURITY CLASSIFICATION
☒ UNCLASSIFIED/UNLIMITED ☐ SAME AS RPT ☐ DTIC USERS	Unclassified
22a NAME OF RESPONSIBLE INDIVIDUAL: Professor Yogendra Joshi	22b TELEPHONE (Include Area Code): (408) 646-3400; 22c OFFICE SYMBOL: 69JI

DD FORM 1473, 84 MAR 83 APR edition may be used until exhausted. All other editions are obsolete.

Approved for public release; distribution is unlimited

Natural Convection from an Array of Rectangular Protrusions in an Enclosure Filled with Dielectric Fluid: Effects of Boundary Conditions, Fluid Prandtl Number, and Selective Component Powering.

by

Mark E. Powell
Lieutenant, United States Navy
B.S., University of Oregon, 1978

Submitted in partial fulfillment of the
requirements for the degree of

MASTER OF SCIENCE IN MECHANICAL ENGINEERING

from the

NAVAL POSTGRADUATE SCHOOL

September 1989

ABSTRACT

An experimental investigation has been conducted to further examine natural convection immersion cooling of a three by three array of heated protrusions in a rectangular chamber filled with dielectric fluid. Each rectangular protrusion geometrically modelled a 20 pin dual-inline-package. Input power to each component varied from 0.1 to 3.0 W..

The purpose of this study was to examine the effects of the following parameters for the range of power levels selected:

1). Top and bottom boundary temperatures.

2). Selective powering of components.

3). Changes in the fluid Prandtl number.

The data were obtained as component surface temperatures. These were subsequently presented in terms of appropriate non-dimensional parameters. As part of the overall investigation, flow visualization results are also presented for selected conditions.

TABLE OF CONTENTS

LIST OF SYMBOLS

Symbol	Description	Units
A	Area	m^2
A_{total}	Total Exposed Surface Area	m^2
c_p	Specific Heat	J / Kg °C
emf	Thermocouple Voltage	mV
g	Acceleration due to Gravity	m / s^2
Gr_f	Flux-based Grashof Number	Dimensionless
Gr_t	Temperature based Grashof Number	Dimensionless
h	Heat Transfer Coefficient	W / m^2 °C
k_f	Fluid Thermal Conductivity	W / m °C
L	Characteristic Length	m
L1	Component Length in the Vertical Direction	m
L2	Summation of the Ratios of the Component Fluid Exposed Areas to their Perimeters	m
Nu	Nusselt Number	Dimensionless
Nu1	Modified Nusselt Number with with Length Scale L1	Dimensionless
Nu2	Modified Nusselt Number with with Length Scale L2	Dimensionless

Pr	Prandtl Number	Dimensionless
Q_{in}	Power Input to the Heaters	W
Q_{loss}	Rate of Loss by Conduction	W
Q_{net}	Net Power Dissipated by the Heater	W
R_c	Total Thermal Resistance	°C/ W
R_p	Resistance of the Precision Resistor	Dimensionless
Ra_f	Flux-based Rayleigh Number	Dimensionless
Ra_t	Temperature based Rayleigh Number	Dimensionless
T_{avg}	Average of Component Surface Temperature	°C
T_{back}	Back Surface Temperature of the Substrate	°C
T_{film}	Film Temperature	°C
T_{sink}	Average Temperature of the Heat Exchangers	°C
U	Uncertainty Value	Various
V_{in}	Input Voltage	Volts
V_h	Voltage Across the Heaters	Volts
α	Thermal Diffusivity	m^2 / s
β	Thermal Expansion Coefficient	1 / °C
ρ	Density	Kg / m^3
υ	Kinematic Viscosity	m^2 / s

I. INTRODUCTION

A. DESCRIPTION OF THE PROBLEM

The final constraint for the continuing development of future generations of high speed, very large scale integration (VLSI) technologies may simply be the lack of effective heat dissipation. In order to meet acceptable system reliability criteria, junction temperatures of modern electronic components must be maintained below 125° C. For every 20° C decrease in junction temperature, the long term reliability improves on the order of 50% [Ref. 1].

Several solution options have been proposed and described in detail [Ref.2&3]. However, in the advent of the 1990's, "Super Chips" powered to 50 W with respective heat fluxes ranging from 50-250 W/cm^2 will saturate the capabilities of forced air cooling technologies [Ref. 4]. Therefore, applications of direct immersion cooling have been the focus of several experimental and computational studies in recent years; Simons and Moran (1977); Bar-Cohan (1983); Simons and Chu(1985); and Joshi et. al.(1989). Single Phase liquid cooling may in general involve natural, mixed or forced convection. Natural convection in dielectric fluids as a cooling mechanism promises to be a potentially attractive technique for thermal control of micro-electronic components/systems. Desirable characteristics include, attainable high heat transfer rates, low noise, high reliability, and simplicity of design. Unfortunately, direct immersion cooling applications have only been limited to mixed or forced convection in a Cray-2 Supercomputer.

B. STUDIES OF NATURAL CONVECTION COOLING OF ELECTRONIC DEVICES

Direct immersion cooling of discrete heat source using both forced and natural convection was first examined by Baker [Ref. 5]. Air, Freon 113 (Prandtl number (Pr) = 3.9) and Dow Corning #200 silicone dielectric liquid (Pr = 126) were used. Results indicated that natural convection direct liquid cooling was three times more effective than natural air convection cooling. Also, the analysis showed that the heat transfer coefficient isapproximately proportional to the cube root of the reciprocal of viscosity. Consequently, the use of a lower viscosity fluid would increase the heat transfer coefficient significantly.

In a following investigation, Baker [Ref. 6] demonstrated that liquid immersion techniques can effectively cool small heat sources. The study showed the effect of heat source size on the heat transfer coefficient with both natural and forced convection in two different liquids. Results indicated an order of magnitude increase in the heat transfer coefficient as heat source size decreased from 2.0 to 0.01 cm^2.

Park and Bergles [Ref. 7] examined natural convection with discrete flush mounted protruding heaters of 5 and 10 mm height and widths in the range of 2-70mm, in water and Freon 113. This study indicated that the heat transfer coefficient increased with decreasing width, with the effect greater in Freon 113 than water. Data also indicated, that the heat transfer coefficients, for various array configurations, were higher in the upper heaters than the lower heaters, and as the

distance between the heaters increased so did the heat transfer coefficients. Additionally, heat transfer coefficient for a single protruding heater was about 15% higher than that for a flush surface.

Keyhani et. al. [Ref. 8] investigated the buoyancy driven flow and heat transfer in a vertical cavity with discrete flush heat sources on one vertical sidewall. The enclosure chamber configuration had 11 alternatively unheated and flush mounted rows of isoflux strips. Two immersion coolants were used, water and ethylene-glycol (Pr = 150).

Chen et. al. [Ref. 9] investigated natural convection heat transfer in a liquid filled rectangular chamber with 10 protruding heaters from one vertical wall. The top chamber surface was maintained at a uniform temperature and acted as a heat sink. All other chamber surfaces were unheated. Two fluids, distilled water and ethylene glycol were used as immersion coolants. Results indicated that, at low Rayleigh number, the bottom heater had the highest heat transfer coefficient. At high Rayleigh numbers, the top heater had the highest heat transfer coefficient. Flow visualization was also conducted.

Liu et. al. [Ref. 10] presented a finite difference numerical study of natural convection flow in a rectangular chamber, with a 3 by 3 array of uniformly heated protrusions mounted on an otherwise adiabatic vertical wall. The enclosure was filled with Fluorinert FC-75 dielectric fluid. The top and bottom were maintained at uniform temperatures while the other boundaries were adiabatic. Results of this numerical study were presented for chamber widths of 18 and 30 mm.

Kelleher et. al [Ref. 11] investigated natural convection flow and heat transfer in a water filled rectangular chamber with a long heater protruding from one vertical insulated wall. Visualizations indicated a dual celled flow structure. The "Buoyancy driven" upper cell accounted for a majority of convective heat transfer. A "shear driven" lower cell was also found, in which the fluid motion arises due to viscous drag from the upper cell.

Lee et. al. [Ref. 12] confirmed the distinct flow patterns by accompanying two dimensional numerical computations.

Joshi et. al [Ref. 13] investigated natural convection cooling of a 3 by 3 array of heated protrusions in a rectangular chamber filled with FC-75 dielectric fluid. Results indicated that at low power levels (0.1 W), flow structure was determined primarily by the thermal Boundary Conditions of the chamber. On increasing the power levels (0.7 to 3.0 W) an upward flow developed adjacent to each column of components. The flow away from the elements showed strong three dimensional time dependent behavior with increasing thermal input. Component surface temperatures were used to arrive at non dimensional heat transfer correlations.

C. OBJECTIVES

This work is a continuation of Thesis research conducted at the Naval Postgraduate School. Knock [Ref. 14] studied the effect of the location of a single protruding heater using water in an enclosure. Pamuk [Ref. 15] first studied the heat transfer characteristics of a nine protrusion array immersed in a dielectric fluid in an uninsulated enclosure. Hazard [Ref. 16] investigated natural convection liquid cooling of a vertically oriented simulated component array with and without a

shrouding wall. Benedict [Ref. 17] arranged a horizontally oriented three by three simulated array that investigated various power level inputs, flow visualization, and correlation of data using Nusselt and Rayleigh numbers. Finally, Torres [Ref.18] re-oriented the three by three simulated component array vertically and followed up on Benedicts' work.

Investigation objectives are five fold:

1). Examine the effects of different chamber top and bottom surface Boundary Conditions.

2). Detailed investigation of the effects of various Prandtl number dielectric fluids.

3). Determine effects of selectively powered components.

4). Investigation to the plausibility of determining a single correlation for all data.

5). Flow Visualization

II EXPERIMENTAL SET UP

A. APPARATUS

This study is a continuation of past experiments conducted at the Naval Postgraduate School: Knock [Ref. 14]; Pamuk [Ref. 15]; Hazard [Ref. 16]; Benedict [Ref. 17]; and Torres [Ref. 18]. The purpose of this investigation is to further examine natural convection heat transfer from a 3 by 3 element array of simulated electronic components. The specific aspects investigated were: (i) the effect of fluid Prandtl number on heat transfer; (ii) the effect of varying the top and bottom surface boundary conditions; and (iii) Component temperatures resulting from selective powering.

The experimental enclosure (figure 2.1) is described in detail in Torres [Ref 18]. It was made of 19.1 mm thick plexiglass with the following dimensions:

Length 241.1 mm

Height 152.0 mm

Width 120.7 mm

A 3 by 3 vertical array of discrete protrusions was mounted on a plexiglass substrate. The protrusions simulated an array of 20 pin - dual - inline packages with the following dimensions:

Length 24 mm

Height 6 mm

Width 8 mm

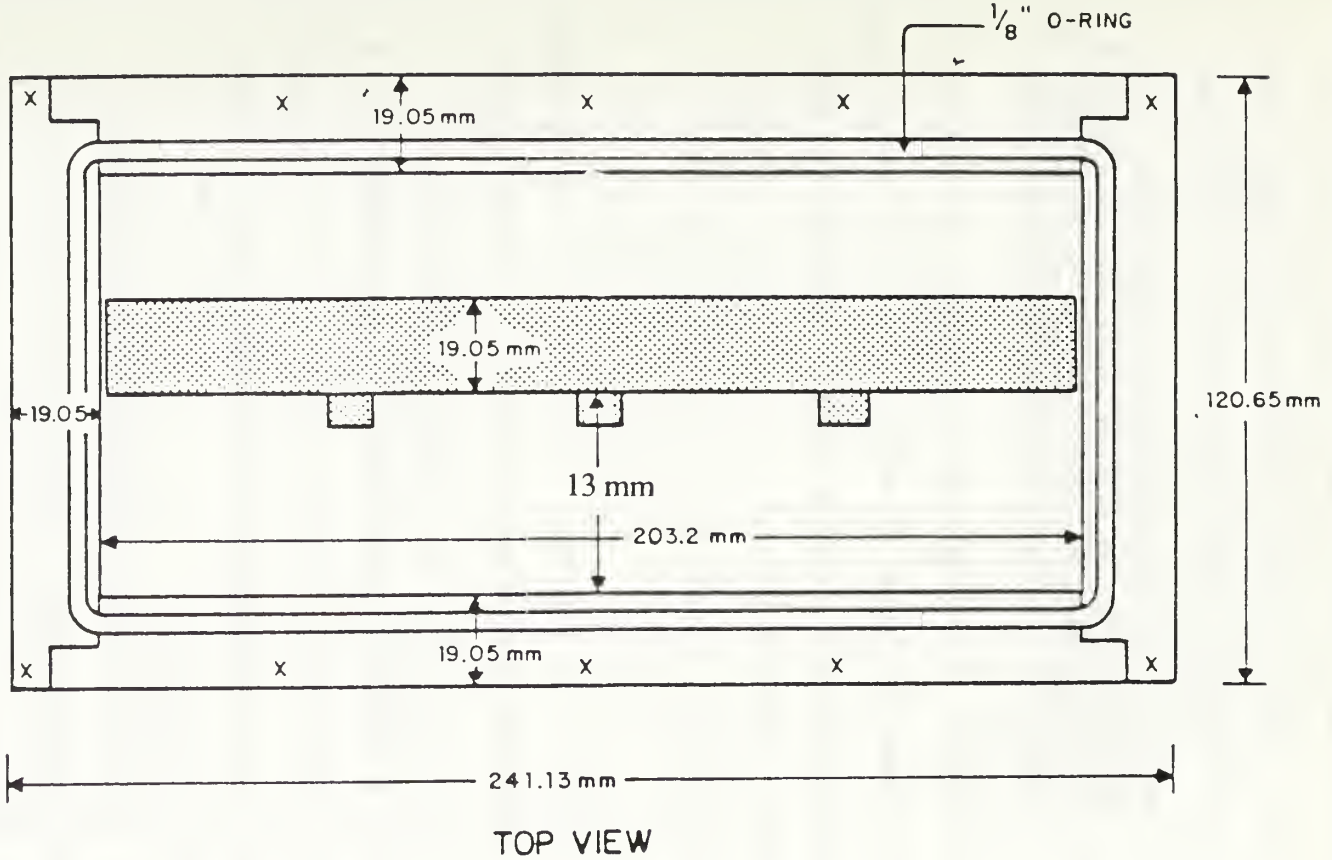

Figure 2.1 **Chamber Assembly for the Vertical Arrangement**

The component dimensions are identical to those investigated by Liu et. al. [Ref 10], Pamuk [Ref. 16] , Benedict [Ref. 17], and Torres [Ref. 18] in order to enable comparisons of experiments and numerical finite difference computations. The components were oriented with their largest dimension being vertical (figure 2.2), with the plexiglass surface containing the protrusions forming a vertical boundary the dielectric inert fluid.

The top and bottom surfaces of the chamber are 3 mm thick Aluminum plates allowing almost uniform surface temperature. In order to maintain the prescribed temperatures, two heat exchangers with individual chilled water circulation baths are attached. Modifications (figure 2.3) were made to the top heat exchangers' inlet and outlet headers described in Benedict [Ref. 17] to allow better flow distribution of coolant.

The protrusions were heated using foil heaters attached to the component bases using a high thermal conductivity epoxy (Omega Bond 101). The heating elements contains a network of Iconel foil mounted on a Kapton backing, and were powered by a 0-40 Volt 0-1 Amp D.C. power supply. The strip heaters were connected in series with 2 Ohm precision resistors. This allowed the measurement of the current. The current was multiplied by the strip heater measured voltage to compute the component power input.

Temperatures at the center of each exposed protrusion face were determined using 0.127 mm diameter embedded Copper Constantan thermocouples (figure 2.4). All thermocouples were connected to a Hewlett-Packard Data Acquisition System (HP-3497) controlled by a Hewlett-Packard micro-computer (HP-9826) shown in Figure 2.5.

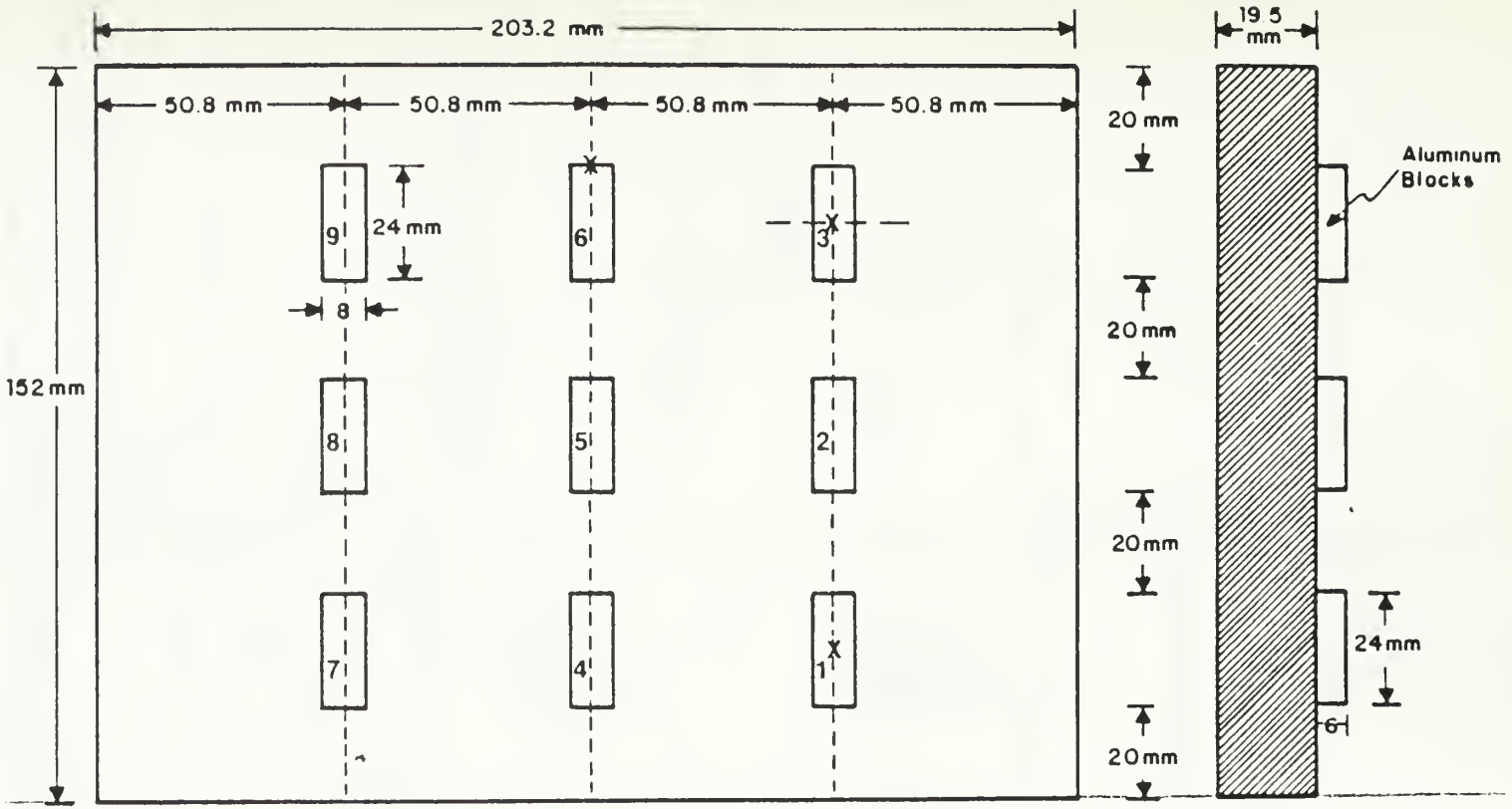

Figure 2.2 **Substrate with Vertical Component Orientation**

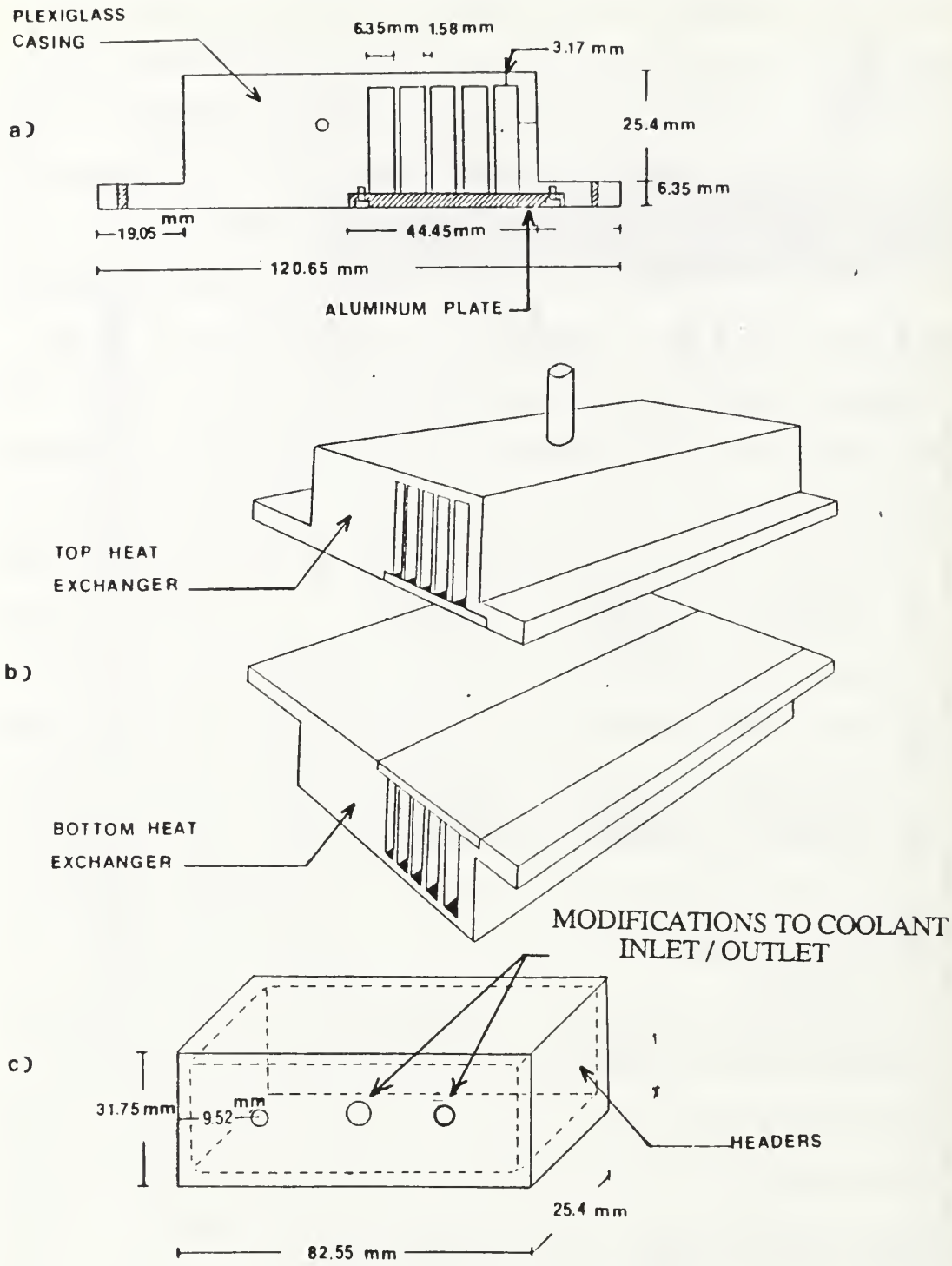

Figure 2.3 **Heat Exchangers**
(a) Cross Sectional View; (b) Isometric View;
(c) Inlet and Outlet Headers

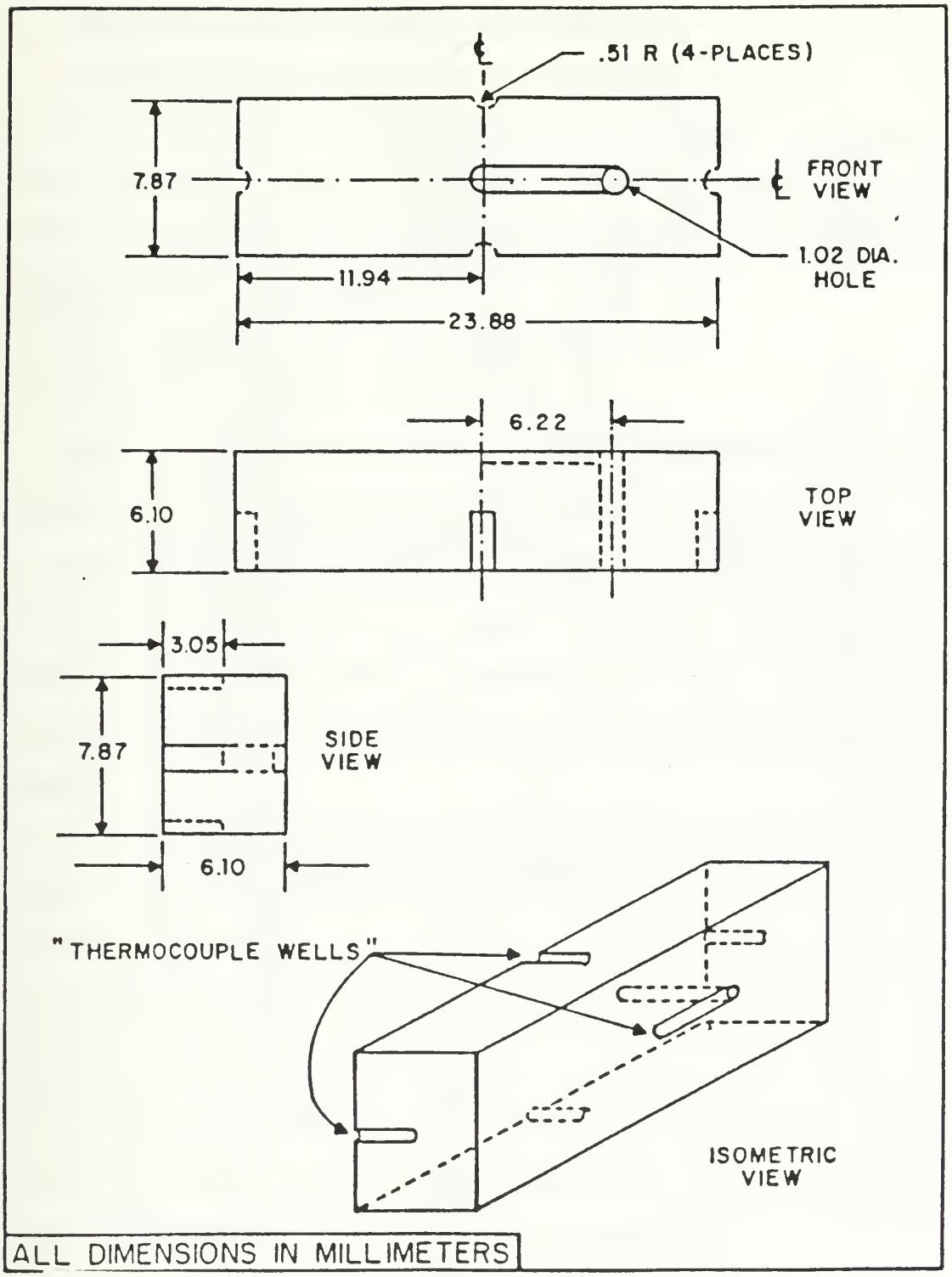

Figure 2.4 **Heating Element and Thermocouple Locations**

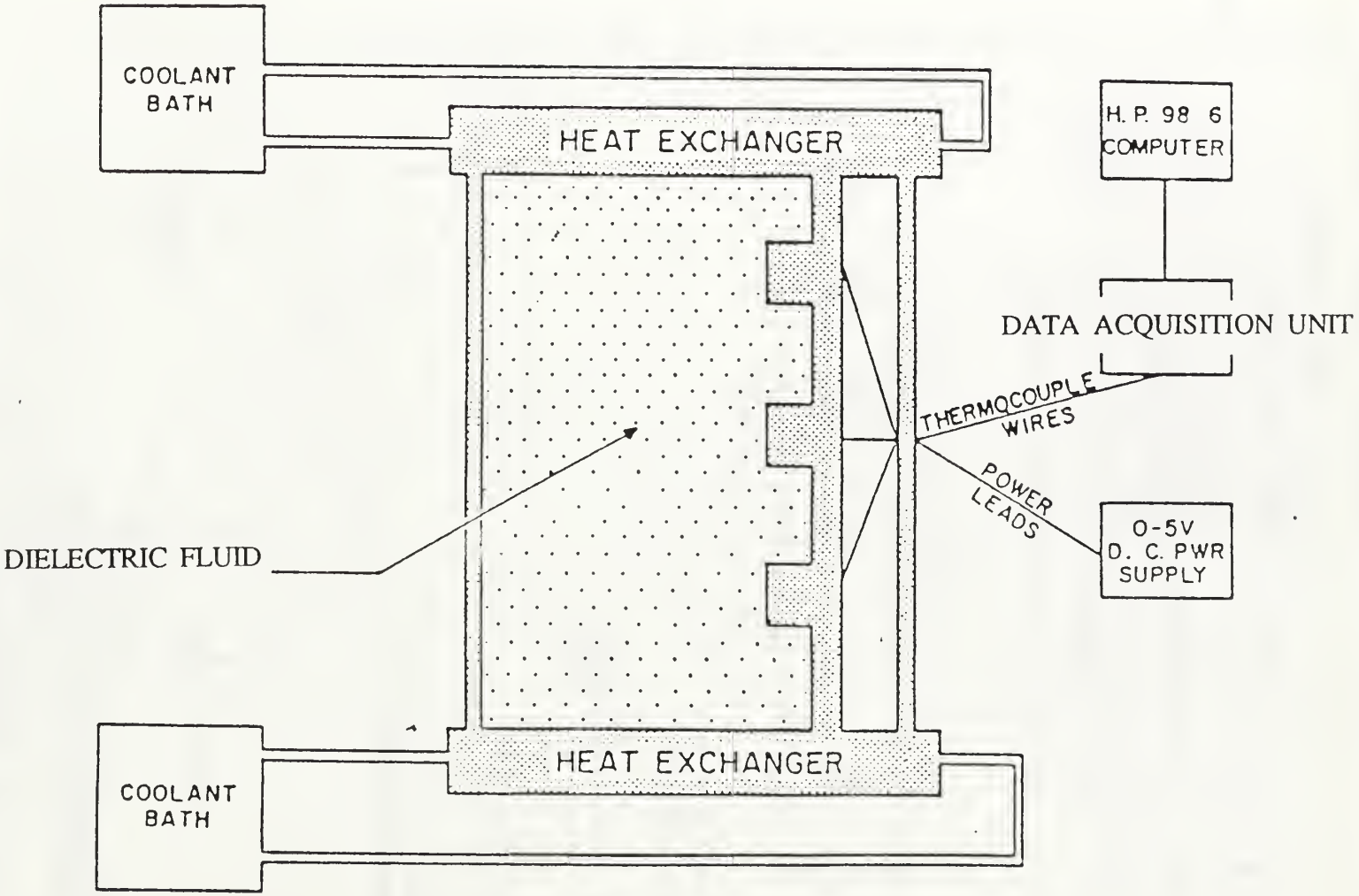

Figure 2.5 **Schematic of Entire Assembly**

B. APPARATUS PREPARATION PROCEDURE

As delineated in Benedict [Ref. 17], once the apparatus was sealed, the chamber was filled with the desired dielectric fluid by using the attached reservoir assembly. It was essential to manipulate the chamber to eliminate the formation of air bubbles within the chamber. The heat exchangers were then independently adjusted and maintained to the desired temperature.

C. DATA ACQUISITION PROCEDURE

Prior to energizing the components, a trial scan was made each time to verify proper operation of all component and heat exchanger thermocouples.

Once the trial run was satisfactorily completed, the desired component power level was set on the power supply. Steady state conditions were assumed when the thermocouple outputs varied by a maximum of 0.5° C, with the majority varying by less than 0.2° C during three successive scans at 15-30 minute time intervals.

Time needed to achieve steady state increased with the viscosity and Prandtl number of the dielectric fluid. For dielectric FC-75 ($Pr \approx 30$) it took approximately 3-5 hours to achieve steady conditions while for higher viscosity dielectric FC-71 ($Pr \approx 1400$) a minimum of 8 hours was needed to achieve steady state conditions.

Once steady state conditions were achieved data were recorded and subsequently processed. The thermocouple emf's were converted into temperatures, which were used in generalizing the thermal characteristics described next.

The Data Acquisition software program ACQUIRE was the same as used by Pamuk [Ref. 16], Benedict [Ref. 17] , and Torres [Ref. 18] with modifications in the different dielectric fluid properties

D. DATA ANALYSIS

1. Heat Transfer Coefficient

Heat transfer coefficients in this study were calculated based on an average component surface temperature in the following manner:

$$h = Q_{net} / A_{total} (T_{avg} - T_{sink})$$

where

Q_{net} ≡ Net rate of energy transferred to the fluid per element. Calculated as the net input power rate minus the conduction loss through the back of substrate.

A_{total} ≡ Total wetted surface area of a specific electronic component

T_{avg} ≡ The temperature average over the exposed area divided by the five wetted component faces, or mathematically

$$T_{avg} = \sum A_i T_i / \sum A_i$$

T_{sink} ≡ Average heat exchanger temperature

2. Nusselt Number

In order to compare results from this experiment with other studies, a non-dimensional representation of the heat transfer performance, the Nusselt number was defined as:

$$Nu = h L / k_f$$

where

$h \equiv$ Convective heat transfer coefficient

$L \equiv$ Height of each component

$k_f \equiv$ Thermal conductivity of the fluid

we note that the fluid properties were taken as a function of the average film temperature calculated as:

$$T_f = (T_{avg} + T_c) / 2$$

for each component.

3. Rayleigh Number

A non-dimensional Rayleigh number based on temperature was defined for this study to be:

$$Ra_t = Gr_t \ Pr$$

where

Gr_t (Grashof number) $\equiv g \ \beta \ L^3 \ \Delta T / \upsilon^2$

Pr (Prandtl number) $\equiv \upsilon / \alpha$

Using the average surface temperature of the specific component defined previously yields the following Rayleigh number expression:

$$Ra_t = g \ \beta \ L^3 \ (T_{avg} - T_{sink}) / \upsilon \alpha$$

Another Rayleigh number based on the component heat flux was defined as follows:

$$Ra_f = Gr_f \; Pr = g \; \beta \; L^4 \; Q_{net} / k_f \; A_{total} \; \upsilon \; \alpha$$

The use of these relationships is presented in the Sample Calculations and Uncertainty Analysis Sections of the Appendices.

III. RESULTS AND DISCUSSIONS

A. HEAT TRANSFER MEASUREMENTS

The bulk of the present investigation involved heat transfer measurements at various power levels to examine effects of variations in top and bottom surface boundary conditions, fluid Prandtl number, and selective powering of components.

Information on the heat transfer characteristics is presented in terms of appropriate non - dimensional groups. As in Benedict [Ref. 17] and Torres [Ref. 18], we identify the Nusselt number (Nu1) as the inverse of the dimensionless surface dimensional flow vigor parameter (see Appendix A Sample Calculations for derivations).

1. Verification with Earlier Data

The starting point of this experimental study was to reproduce results obtained by Torres [Ref. 18]. Using Dielectric FC-75 and setting the top and bottom surfaces to 10 °C, the resulting heat transfer data are seen in Figure 3.1. The corresponding data from Torres [Ref. 18] are seen in Figure 3.2. Comparing Figures 3.1 and 3.2, good agreement is found for the power levels of 0.1 and 0.7 W.

At 1.1 W we see a somewhat larger spread in the magnitude of the Nusselt number. However, at the higher power levels, results of this investigation again are closer in magnitude. Thus an overall satisfactory agreement was found with a maximum difference of 13 % in the Nusselt number values at any given Rayleigh number.

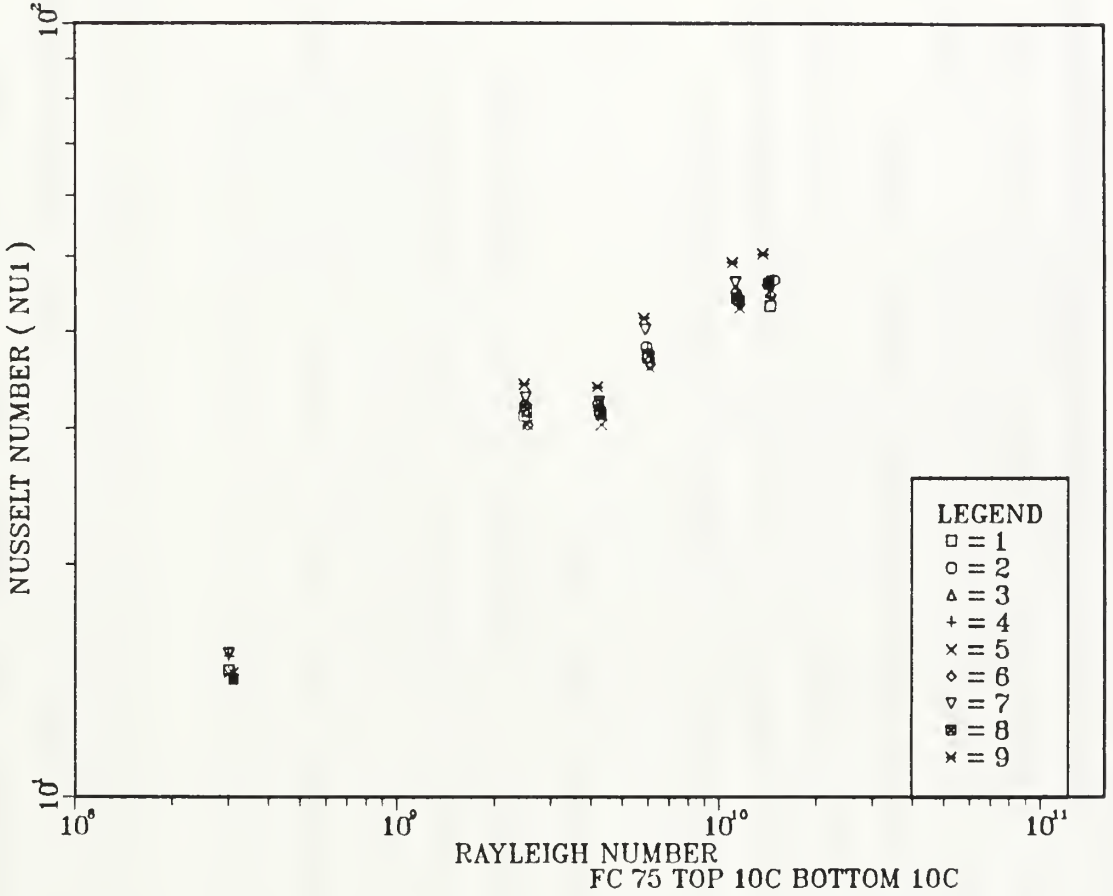

Figure 3.1 **Data Verification Plot of Nusselt (Nu1) vs. Rayleigh (Ra_f) for Chamber Width = 7 mm.**

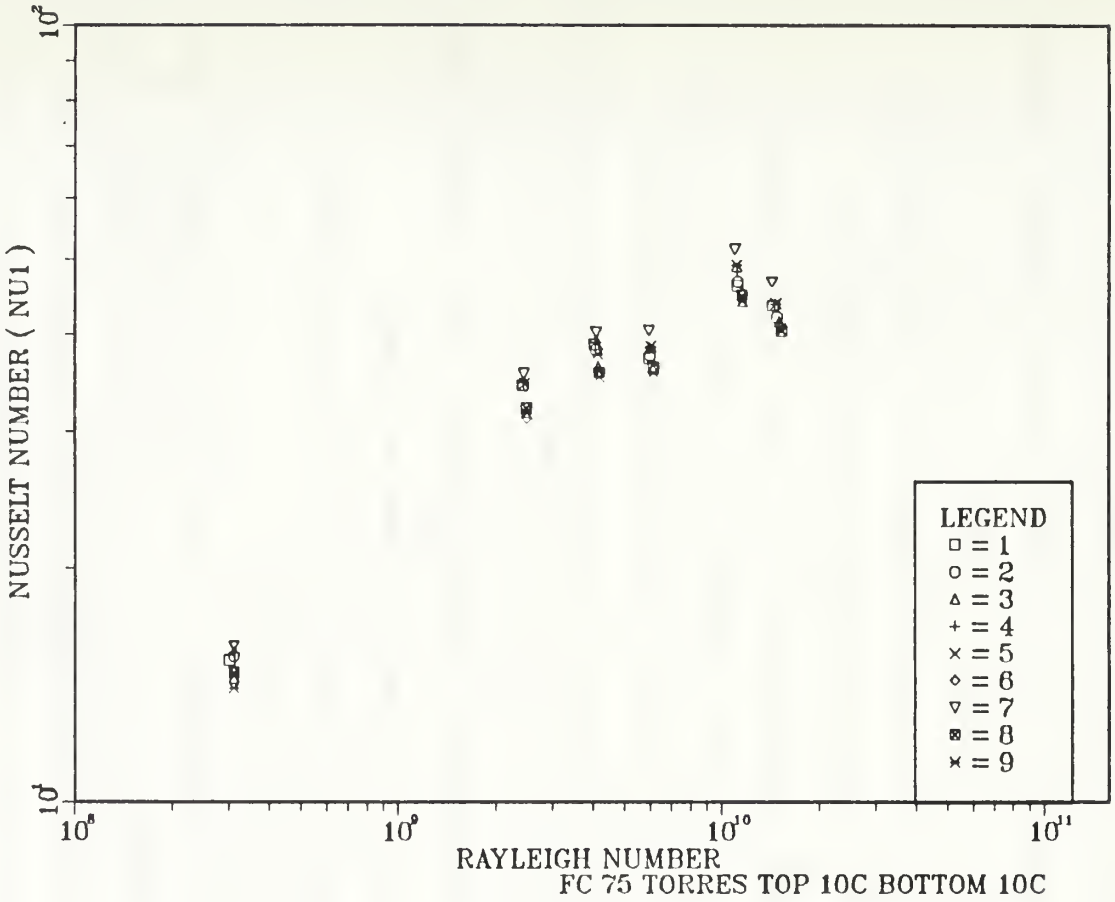

Figure 3.2 **Plot of Nusselt (Nu1) vs. Rayleigh (Ra_f) of the Results from Torres [Ref. 18].**

2. Effects of Varying Top and Bottom Surface Boundary Conditions

One of the objectives of this investigation was to obtain heat transfer data using the same dielectric fluid but varying the enclosure top and bottom surface conditions. In order to examine these effects two sets of plots were generated. The first set (Figure 3.3 to 3.6) determined the difference between the average component surface temperature (T_{avg}) and the average heat exchanger temperature (T_{sink}) versus the power level (Q_{in}). The second set of plots was a non-dimensionalization of the same data and (Figures 3.7 to 3.10) presented the Nusselt number (Nu1) versus the flux based Rayleigh number (Ra_f).

Starting with the Standard case of FC-75 with the top and bottom boundaries set at 15 °C and 10 °C respectively (Figure 3.3), we see that at the lower power levels (0.1, 0.7 W) there is little temperature variation from component to component. However, as the power level increases, the spread in the temperature excess levels of the individual components increase, with the middle column made up of components 4, 5, and 6 (see figure 2.2) has consistently higher temperatures than the other combinations of rows and columns.

The Verification case (Figure 3.4) of 10 °C top and 10 °C bottom boundary temperatures indicated similar trends.

The top 10 °C and the bottom 15 °C case (Figure 3.5) , again show the same general characteristics as the first two cases. However, the magnitudes of the temperature excess levels are now significantly lower. This may be due to the global natural convection flow set up due to the differences between the top and bottom boundaries.

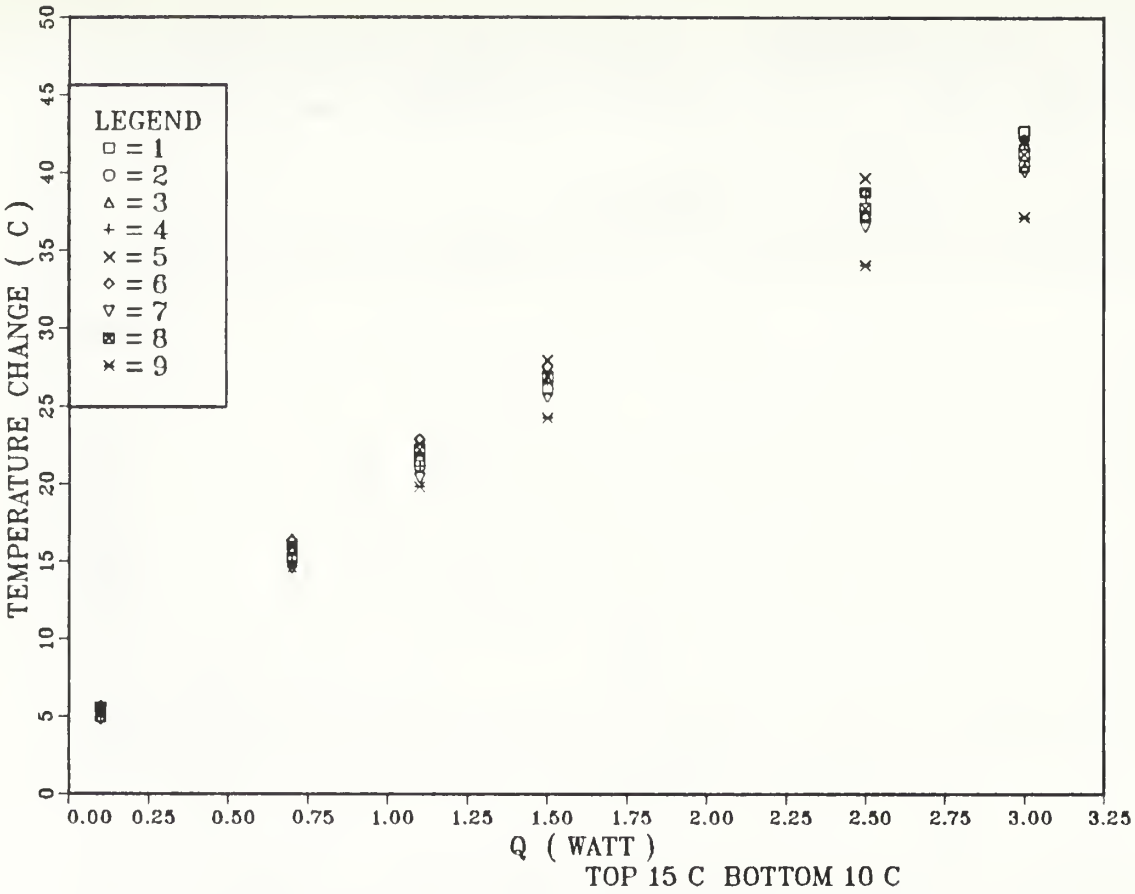

Figure 3.3 **Plot of Temperature Change (ΔT) vs. Input Power (Q) with Top Boundary at 15°C and Bottom Boundary at 10°C (Standard Suface Boundary Conditions).**

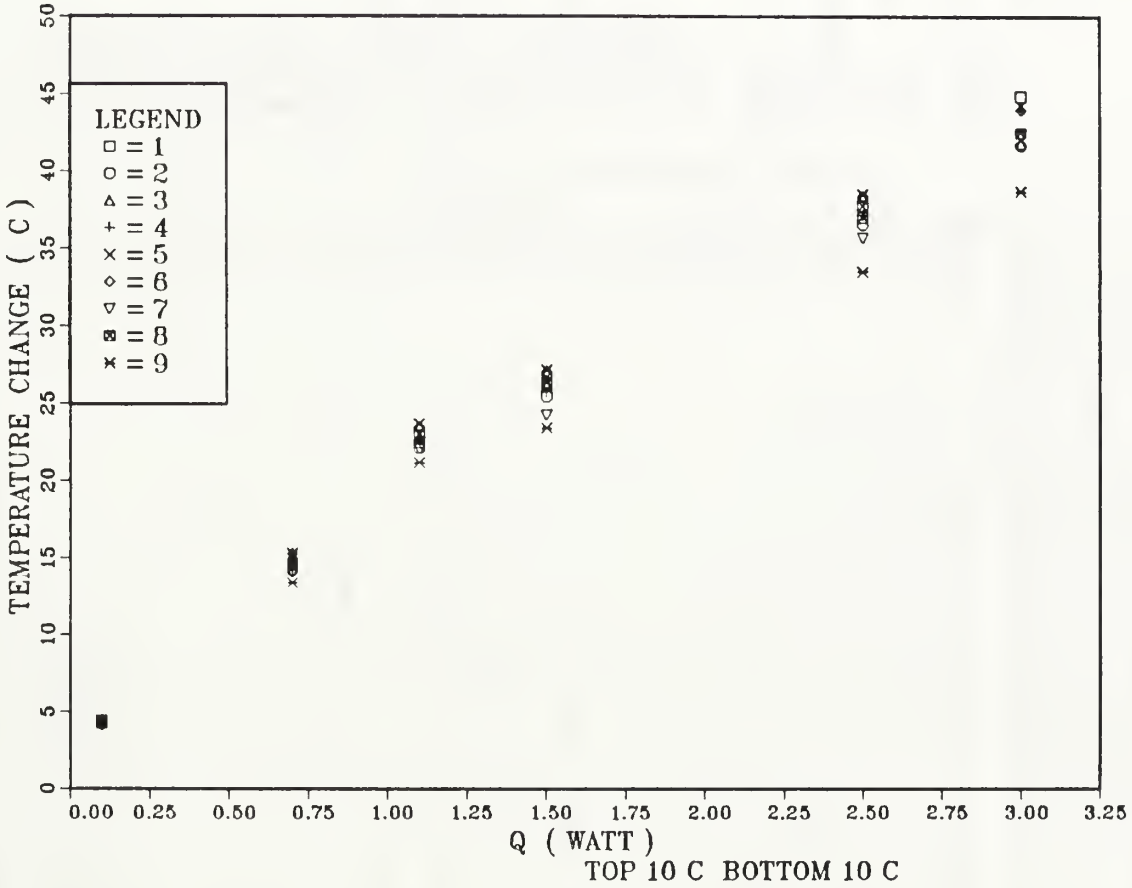

Figure 3.4 **Plot of Temperature Change (ΔT) vs. Input Power (Q) with Top Boundary at 10°C and Bottom Boundary at 10°C (Verification Surface Boundary Conditions).**

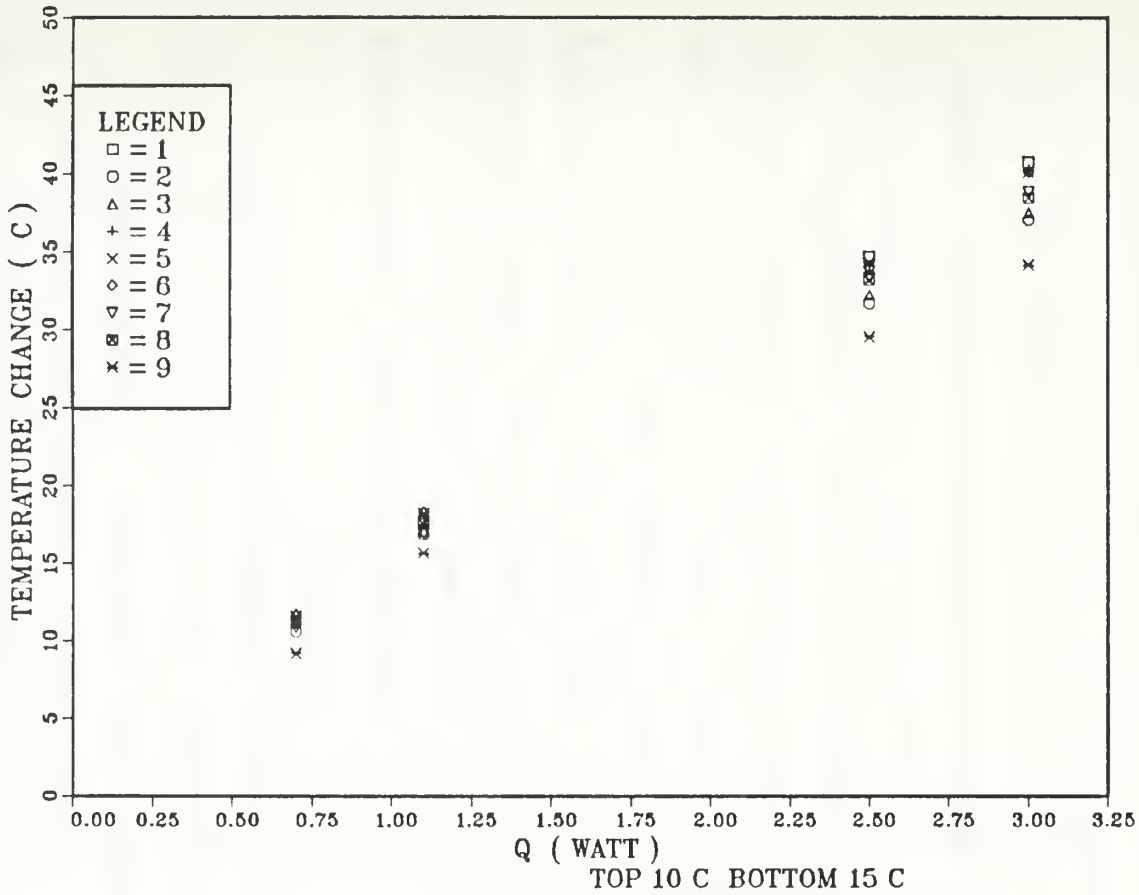

Figure 3.5 **Plot of Temperature Change (ΔT) vs. Input Power (Q) for the Surface Boundary Conditions of 10°C on Top and 15°C on Bottom.**

The last set of measurements was made with the top and bottom surfaces set to an arbitrary "Ambient" temperature (Figure 3.6). Results showed that at the lower power levels (0.1, 0.7, 1.1, 1.5 W) the temperature difference magnitudes of the ambient case were higher than the Standard case and lower at the higher power levels (2.5, 3.0 W).

Reviewing Figures 3.7 to 3.10, an interesting phenomena arises at the higher power levels. Apparently the displayed effects of the boundary conditions are insignificant to the Nusselt / Rayleigh number relationship, since the buoyancy forces produced near the components tend to dominate the circulating flow.

The only major difference in these Figures are the responses at the 0.1 W power level . Evidently the component energization at these levels has only a weak influence on the natural circulation of the dielectric fluid.

The Standard boundary condition case (Figure 3.7), 15°C on the top and 10°C on bottom, presumably shows the effect of a stably stratified colder region that was present throughout the entire chamber. In Figures 3.8 and 3.9, the results of the 0.1 W power level were very similar to the previous case, probably due to a dominant stagnant region of dielectric fluid.

However when comparing the Ambient case (Figure 3.10) with the previous cases, the effect of higher surface boundary temperatures has a significant influence on the magnitude of the Nusselt number at lower input power levels. Apparently for these boundary conditions, the stably stratified region of fluid diminishes, enabling a natural circulation, which results in higher Nusselt numbers.

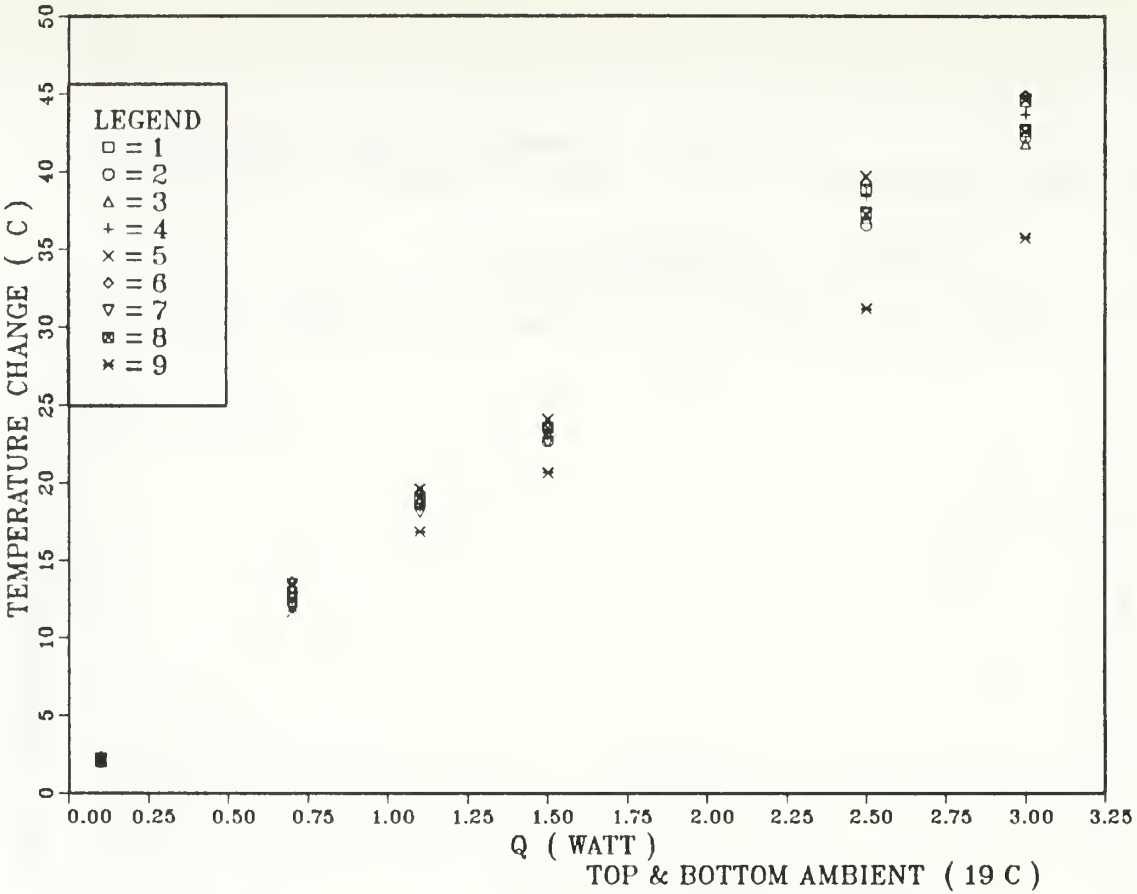

Figure 3.6 **Plot of Temperature Change (ΔT) vs. Input Power (Q) the Top and Bottom Boundaries at 19°C .**

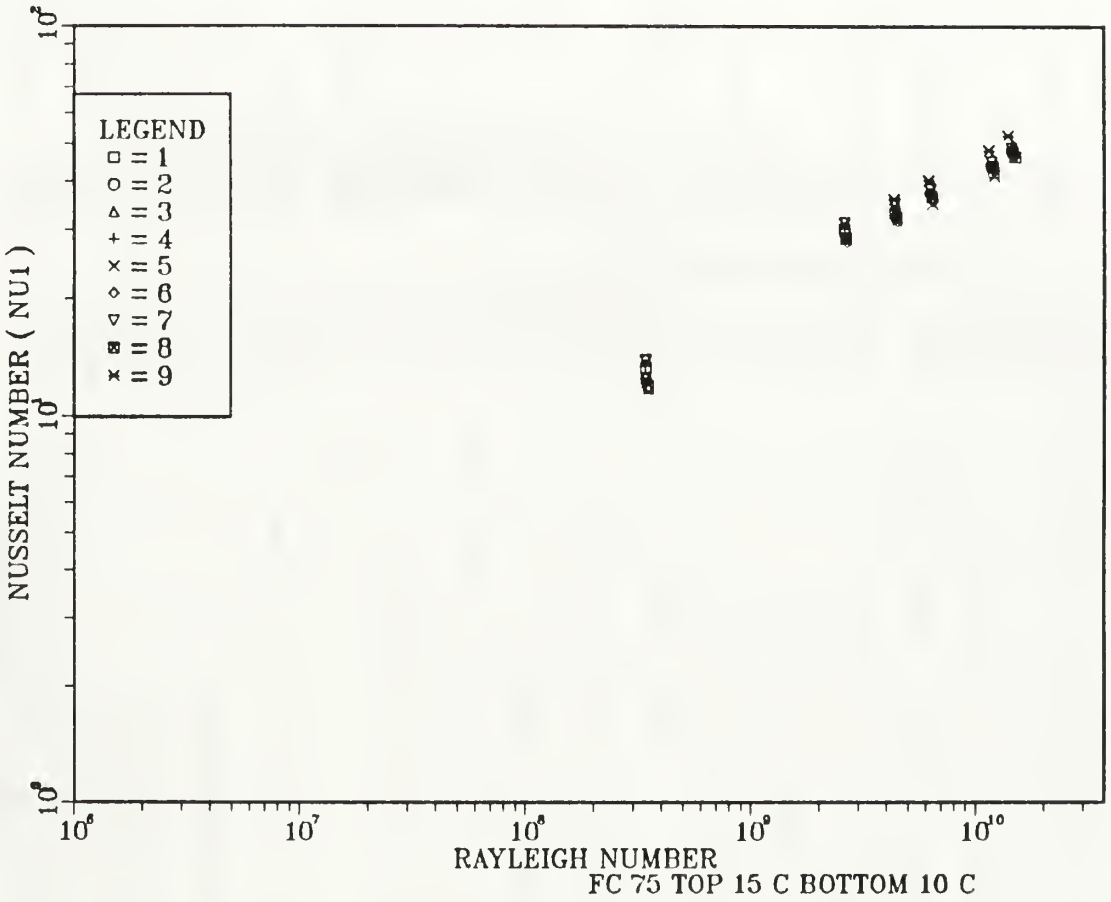

Figure 3.7 **Plot of Nusselt Number (Nu1) vs. Rayleigh Number (Ra_f) for Standard Surface Boundary Conditions.**

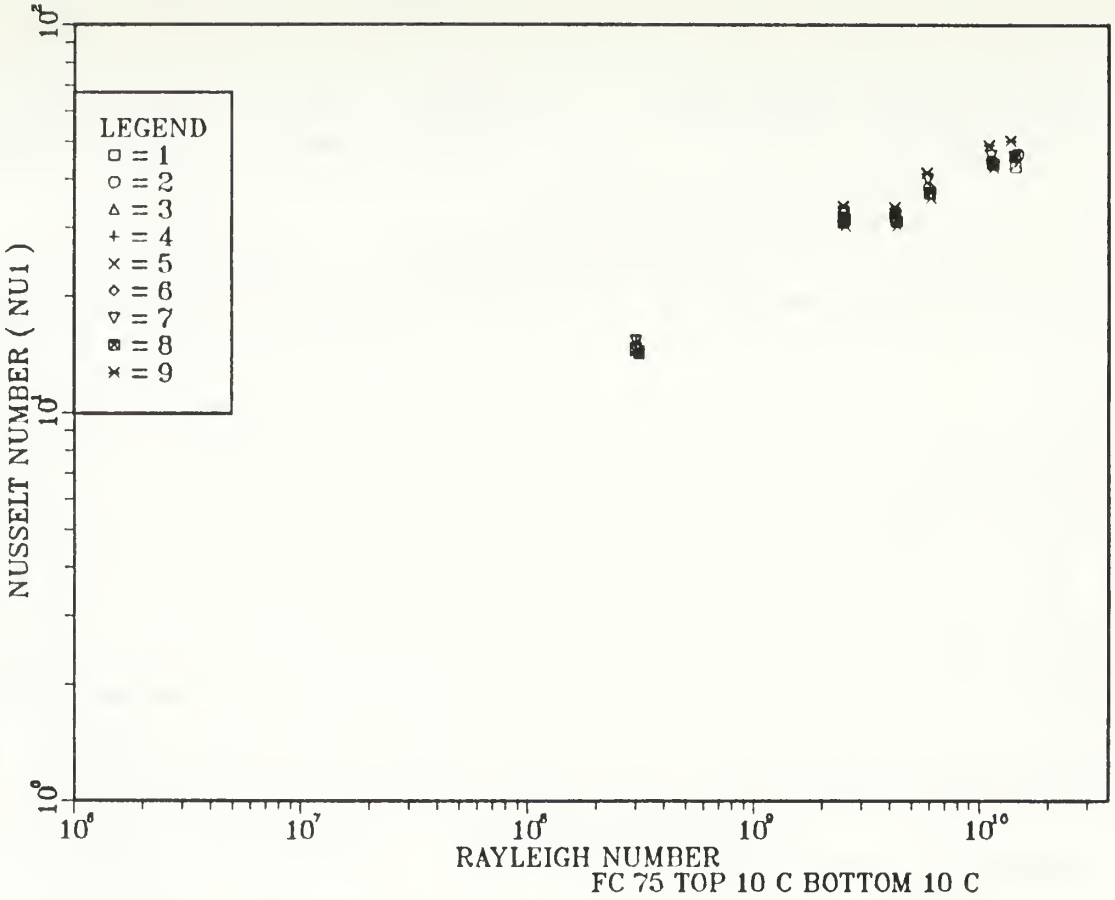

Figure 3.8 **Plot of Nusselt Number (Nu1) vs. Rayleigh Number (Ra_f) for Verification Surface Boundary Conditions.**

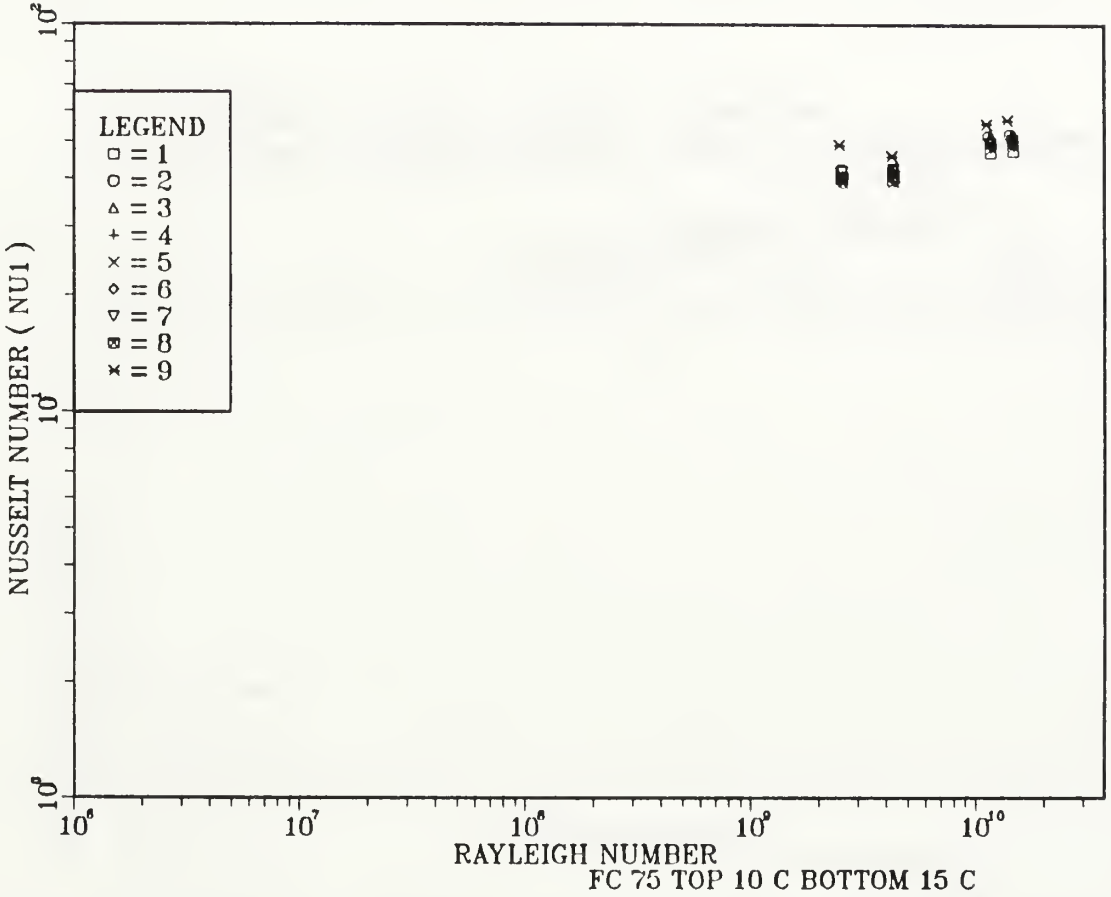

Figure 3.9 **Plot of Nusselt Number (Nu1) vs. Rayleigh Number (Ra_f) for the Surface Boundary Conditions of 10°C on Top and 15°C on Bottom.**

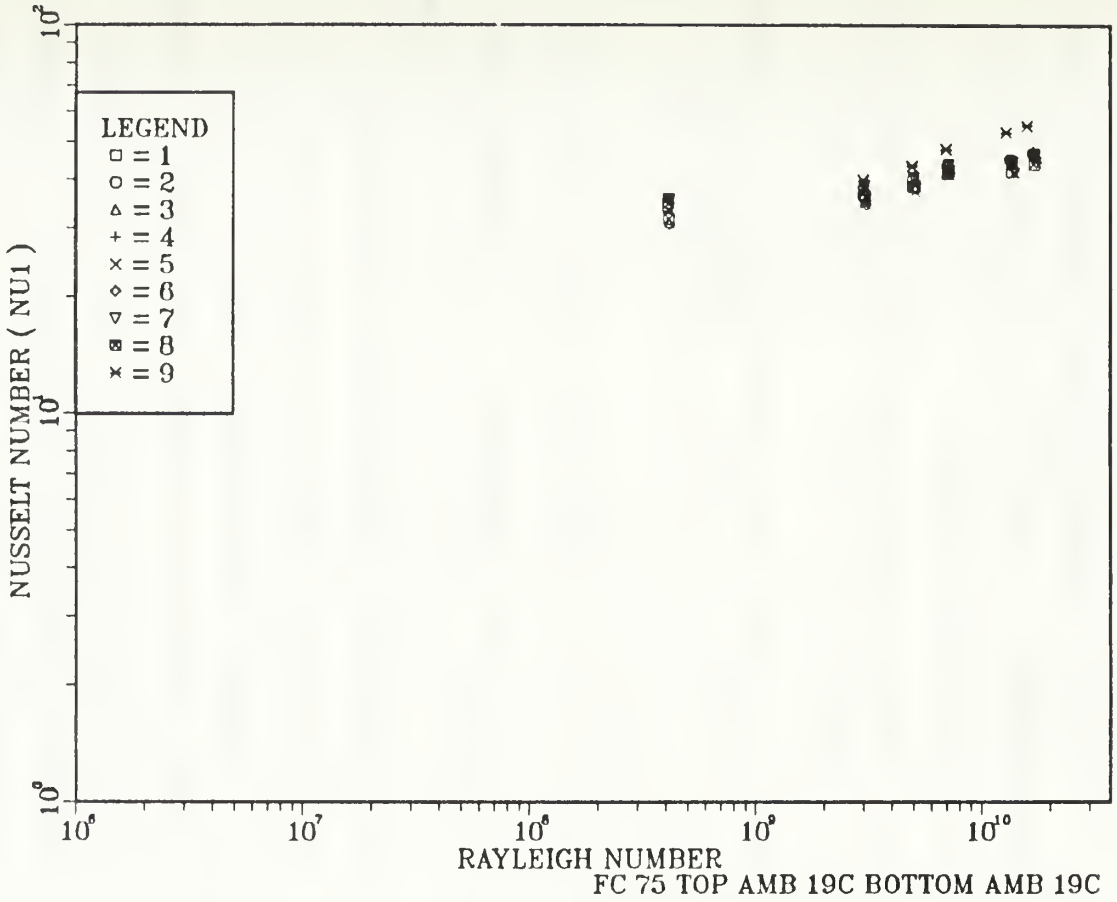

Figure 3.10 **Plot of Nusselt Number (Nu1) vs. Rayleigh Number (Ra_f) for the Ambient (19°C) Surface Boundary Conditions.**

3. Variations in Fluid Prandtl Number

The objective of this part of the overall investigation was to examine the heat transfer characteristics of different dielectric fluids. The thermo-physical properties of the fluids used are provided in Table 1. These values were determined at a temperature of 300 K (Refer to Appendix A Sample Calculations for curve fit equations used at other temperatures). As seen in Table 1, the Prandtl number varies from 24.2 for FC-75 to 1400.5 for FC-71.

Experiments were conducted using the Standard conditions of having the top surface at 15 °C and the bottom at 10 °C.

For FC-75 (Figure 3.11) with a Prandtl number variation of approximately 30 to 25 in a range from 17 - 50 °C, the data indicate almost a single slope except for the lowest power level (0.1 W).

For FC-43 (Figure 3.12) with a Prandtl number variation of approximately 124 to 58 in a range 18 - 50 °C show similar trends. As for FC-75, the lowest power level tends to deviate from the remaining data. As mentioned in the previous section, this maybe due to the chamber boundary conditions which play an important role at lower power levels. At higher power levels, the flow in the vicinity of the component appears to dominate the heat transfer characteristics. Also, in comparison to FC-75, for the same component power levels, the Rayleigh numbers experienced a shift towards the left due to the higher fluid viscosities.

Additional experiments with FC-43 were performed with both boundaries maintained at 15 °C. The results (Figure 3.13) showed little deviation from the

DIELECTRIC FLUORINERT PROPERTIES

(T_{film} = 300 K = 27° C)

	FC 75	FC 43	FC 71
r (kg / m^3)	1759.0	1854.5	1941.9
k (W / m K)	0.0629	0.0663	0.0710
c_p (J / kg K)	1050.9	1050.9	1050.9
υ (m^2 / s)	0.838E-6	2.781E-6	48.726E-6
α (m^2 / s)	34.02E-9	34.04E-9	34.79E-9
β (1 / °C)	1.399E-3	1.176E-3	1.154E-3
Pr	24.62	81.70	1400.5

Table 1. **Comparison of the Fluorinert Dielectric Fluids**

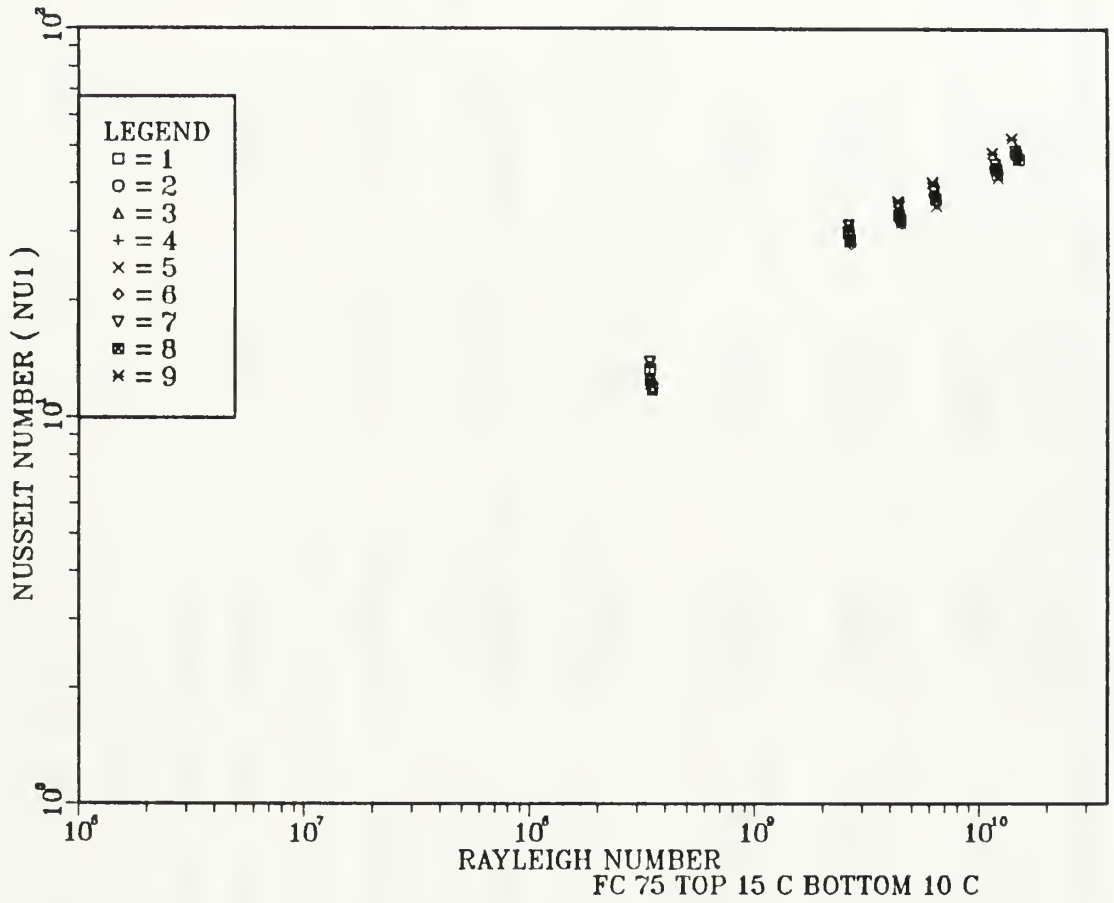

Figure 3.11 **Plot of Nusselt Number (Nu1) vs. Rayleigh Number (Ra_f) for Dielectric FC-75 with Standard Surface Boundary Conditions.**

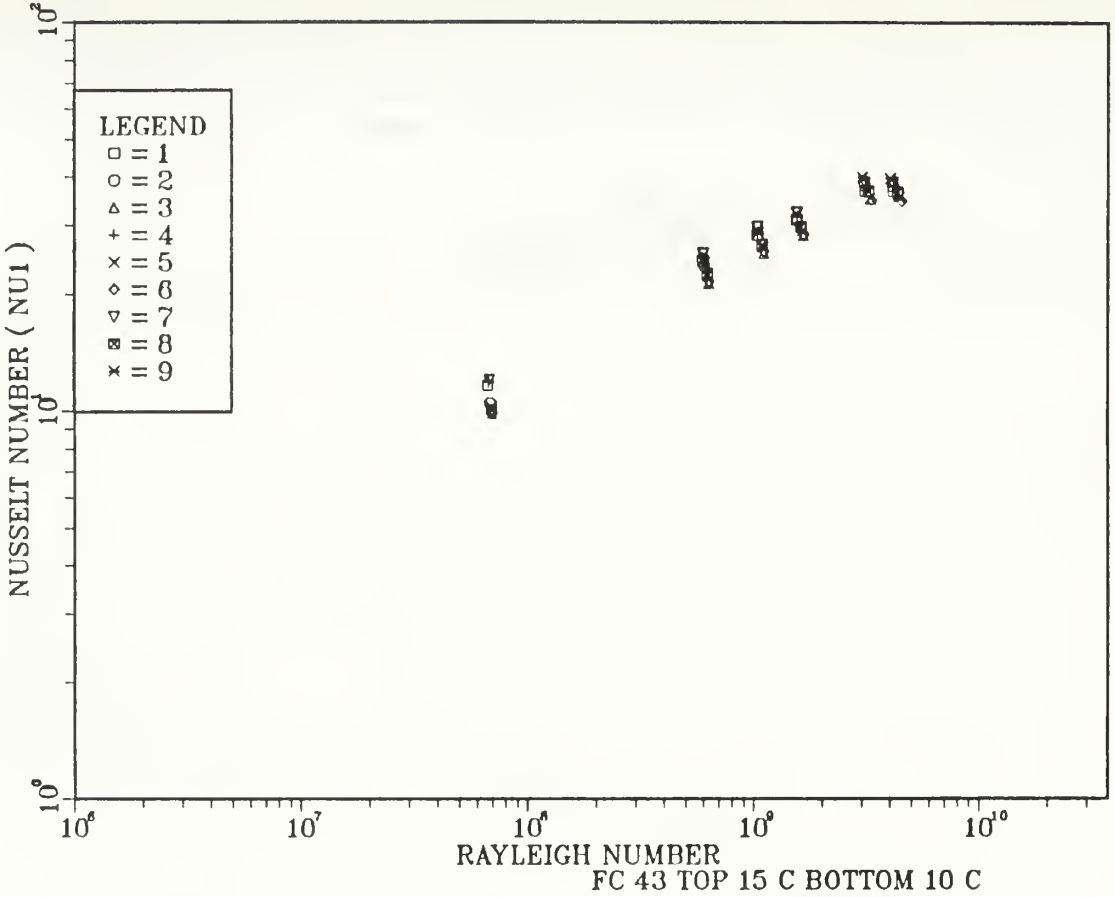

Figure 3.12 **Plot of Nusselt Number (Nu1) vs. Rayleigh Number (Ra_f) for Dielectric FC-43 with Standard Surface Boundary Conditions.**

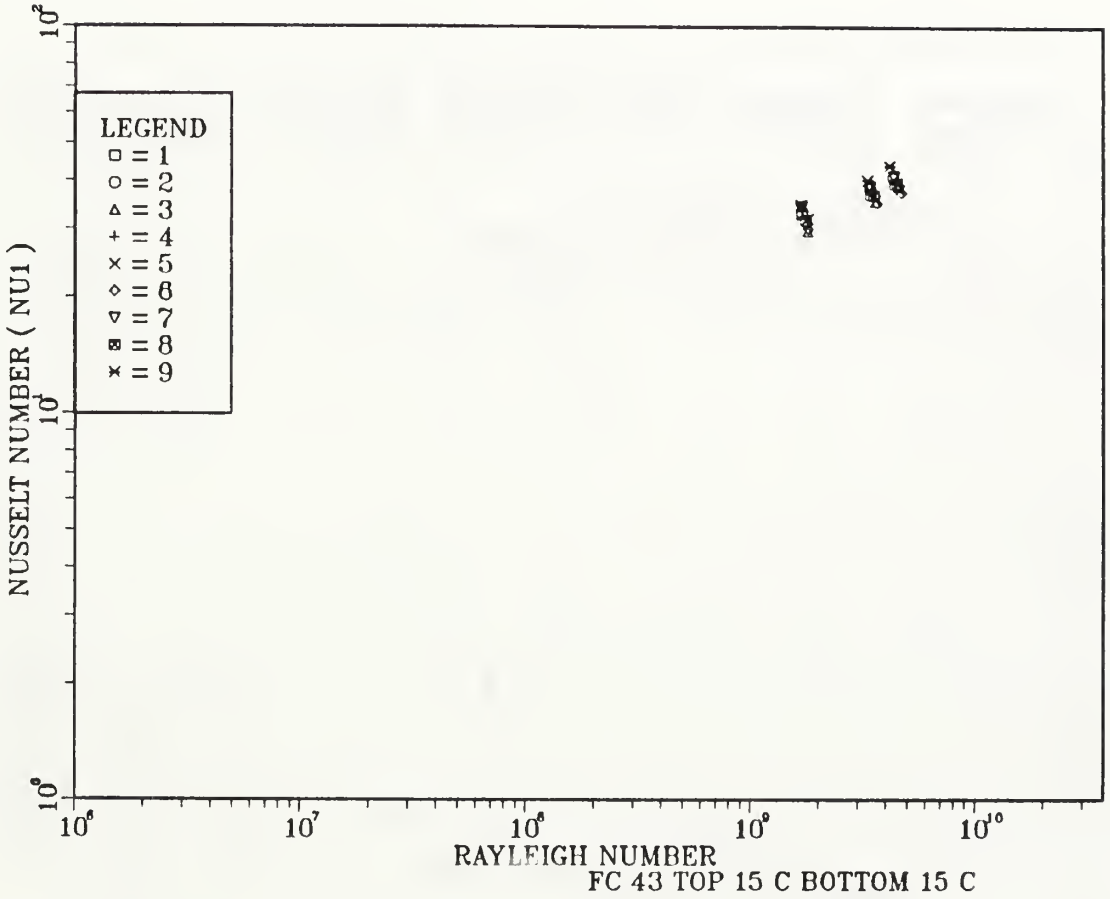

Figure 3.13 **Plot of Nusselt Number (Nu1) vs. Rayleigh Number (Ra_f) for Dielectric FC-43 with Surface Boundary Conditions of 15°C on the Top and Bottom.**

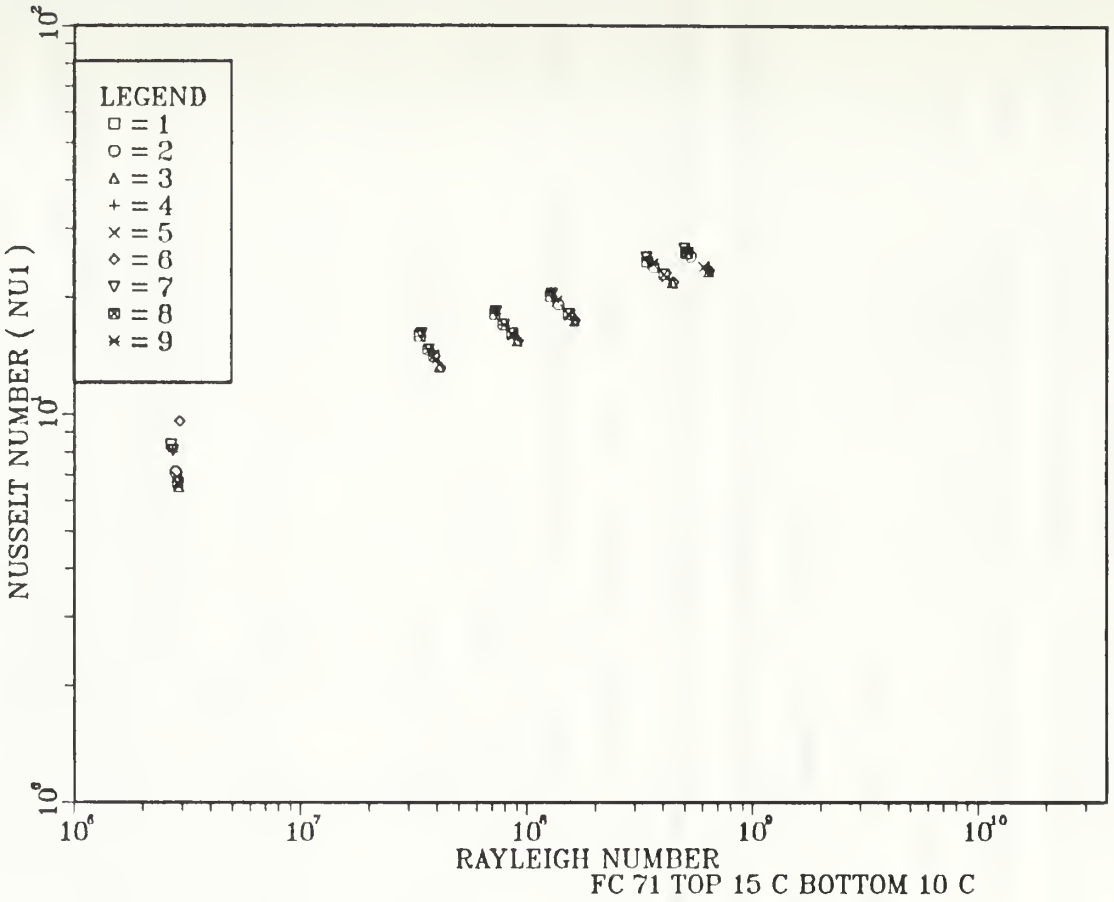

Figure 3.14 **Plot of Nusselt Number (Nu1) vs. Rayleigh Number (Ra_f) for Dielectric FC-71 with Standard Surface Boundary Conditions.**

previous FC-43 case (Figure 3.12). This again demonstrates the effectiveness of the temperature excess in correlating the heat transfer measurements for various combinations of boundary temperatures.

The final fluid was FC-71 (Figure 3.14) with a Prandtl number variation of 2284 to 369 in the range 21 - 85 °C. Comparing these results with FC-75 shows a somewhat smaller slope of the variation. The large increase in fluid viscosity shifts the Rayleigh number to the left by approximately 2 orders of magnitude, at the same power levels.

a. Numerical Correlation of Data

The data for the various Prandtl number fluids for all power levels and the standard boundary conditions were collected and presented in a Log - Log plot of Nusselt (Nu1) and the flux based Rayleigh number (Figure 3.15). The following best fit line was generated to determine the Nusselt number and Rayleigh number relationship at a chamber width of 7 mm:

$$Nu1 = 0.29\ Ra_f^{0.2168} \qquad (3.1)$$

where,

$$2 * 10^6 < Ra_f < 1.5 * 10^{10}$$

$$15 < Pr < 2884$$

which is consistent with the results determined by Benedict [Ref. 17] and Torres [Ref. 18] . However, the differences in the geometry and enclosure dimensions in these determinations should be emphasized.

Benedict [Ref. 17] used a horizontal orientation for the 3 by 3 protrusion array. At a 120 mm by 144 mm by 30 mm chamber width using FC-75 dielectric fluid it was determined that:

$$Nu1 = 0.28\ Ra_f^{0.22} \qquad (3.2)$$

where,

$$10^7 < Ra_f < 2 * 10^8$$

$$15 < Pr < 30.2$$

Torres [Ref. 18] studied the 3 by 3 protrusion array in a vertical configuration with the same chamber size as in the present experiment. The dielectric fluid was FC-75 with the chamber width of 7 mm. The resulting best fit equation was:

$$Nu1 = 0.073\ Ra_f^{0.28} \qquad (3.3)$$

where,

$$3 * 10^8 < Ra_f < 10^{10}$$

$$15 < Pr < 30.2$$

Both Benedict [Ref. 17] and Torres [Ref. 18] carried out measurements with the top and bottom boundary temperatures of 10 °C.

Comparing equations 3.1, 3.2, and 3.3 reveals that moderate differences in chamber width, changes in fluid Prandtl number, and protrusion orientation have only a weak effect on the best fit equation. It must be emphasized, however, that the best fit line does not corresponds to the lowest Nu1 values.

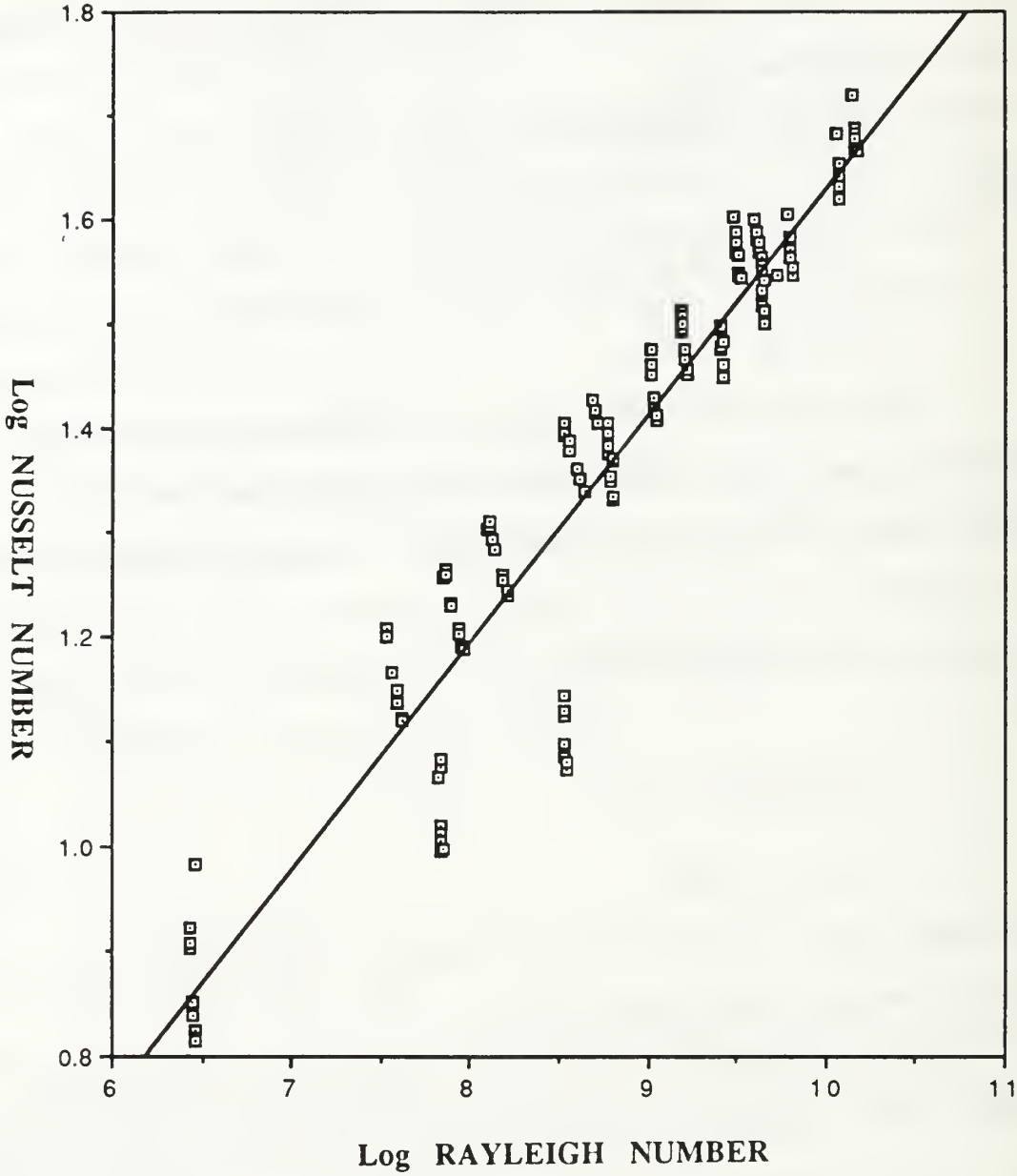

Figure 3.15 Plot of Best Fit Line from the Correlation of Data for Various Prandtl Number Fluids, where,

$$Nu1 = 0.29\ Ra_f^{0.2168}$$

Reviewing the data points that contributed to equation 3.1, shows the greatest derivation from this fit corresponds to the lowest power level (0.1 W), where the enclosure surface boundary conditions are the most significant. When these points are not included in the curve fit, the resulting best fit line seen in Figure 3.16 is given by:

$$Nu1 = 0.49\ Ra_f^{0.1936} \qquad (3.4)$$

4. Selective Powering of Components

This was studied by energizing only one column of protrusions (Components 4, 5, and 6) and in another set of experiments energizing component 5 only. The standard surface conditions were employed with three different dielectric fluids, in most experimental runs. Additional runs were made with FC-75 with ambient (both the top and bottom at 19°C) surface conditions.

The results (Figures 3.17 to 3.20) indicate higher Nusselt number values at a given Rayleigh number, compared to fully powered array. This is expected since the component temperature rise is smaller with partial powering of the array. The highest Nusselt number resulted with the powering of only a single component.

With the single column energized, the lower the position of the component within an column, the higher was the Nusselt number value at the same input power. This is consistent with the numerical study conducted by Liu et. al. [Ref. 19].

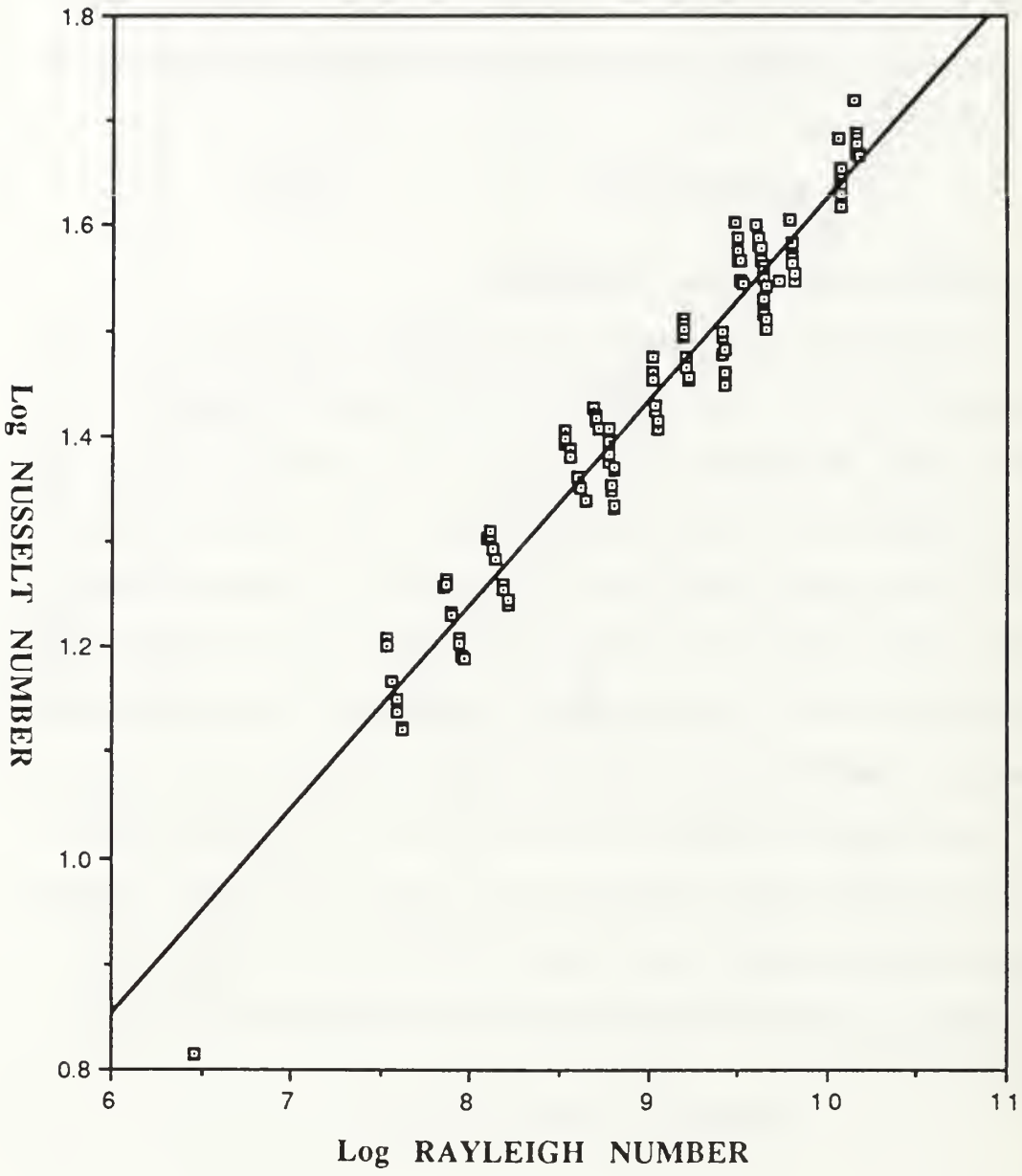

Figure 3.16 **Plot of Modified Best Fit Line, where,**

$$Nu1 = 0.49\ Ra_f^{0.1936}$$

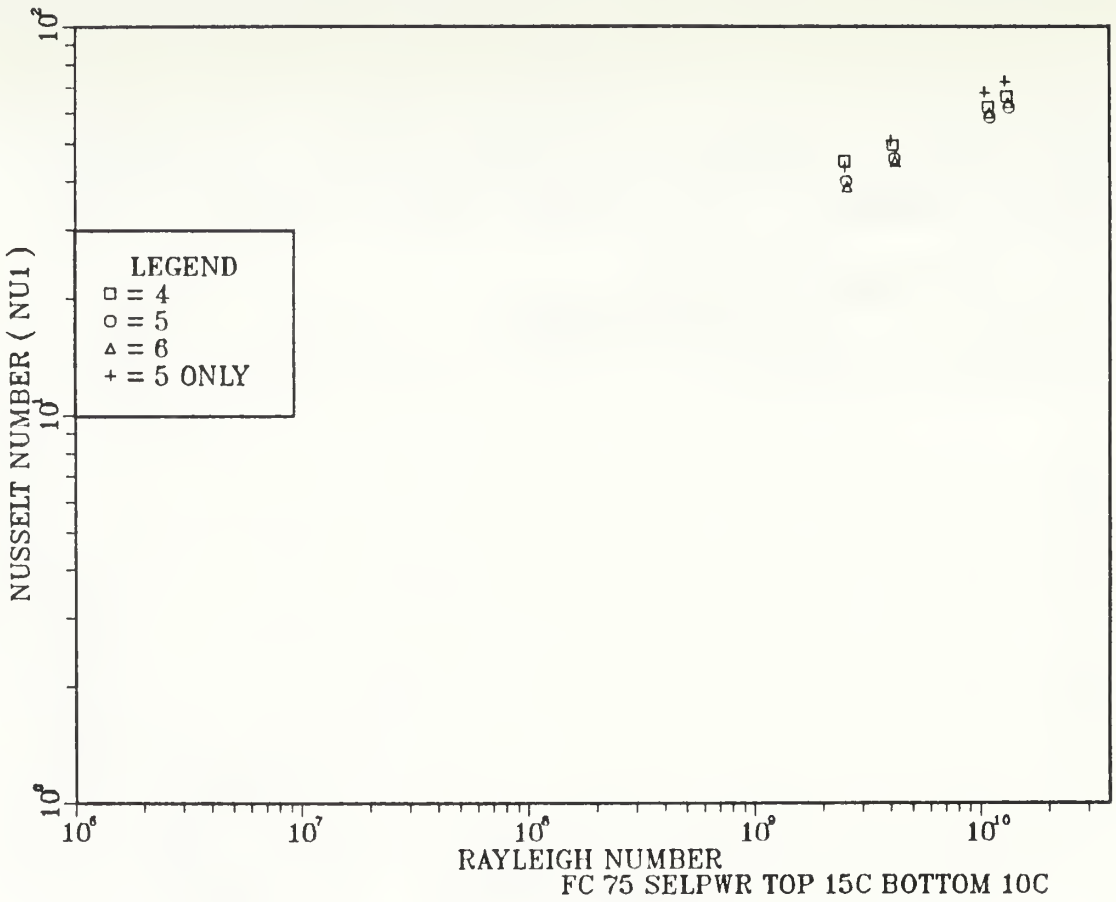

Figure 3.17 **Plot of Nusselt (Nu1) vs. Rayleigh (Ra_f) for Dielectric FC-75 during Selective Powering of Components using Standard Surface Boundary Conditions.**

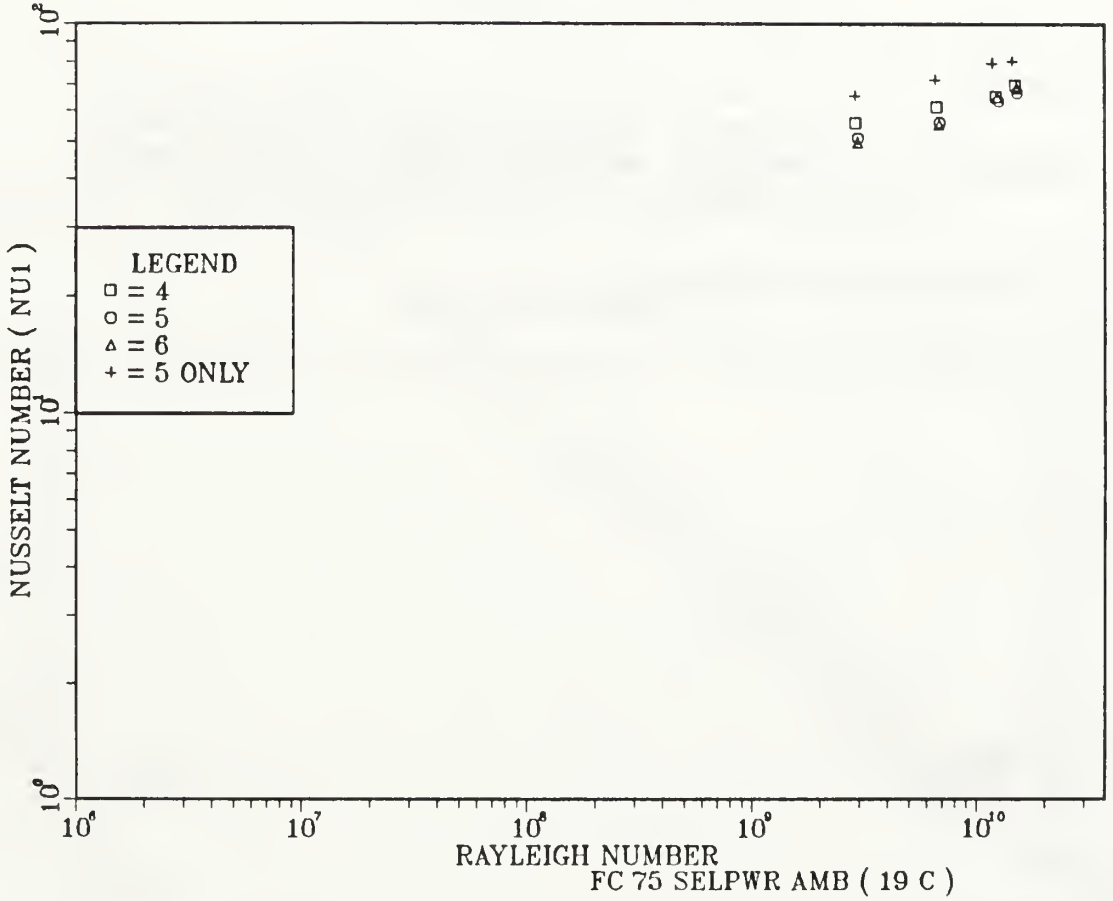

Figure 3.18 **Plot of Nusselt Number (Nu1) vs. Rayleigh Number (Ra_f) for Dielectric FC-75 during Selective Powering of Components using Ambient (19°C) Surface Boundary Conditions.**

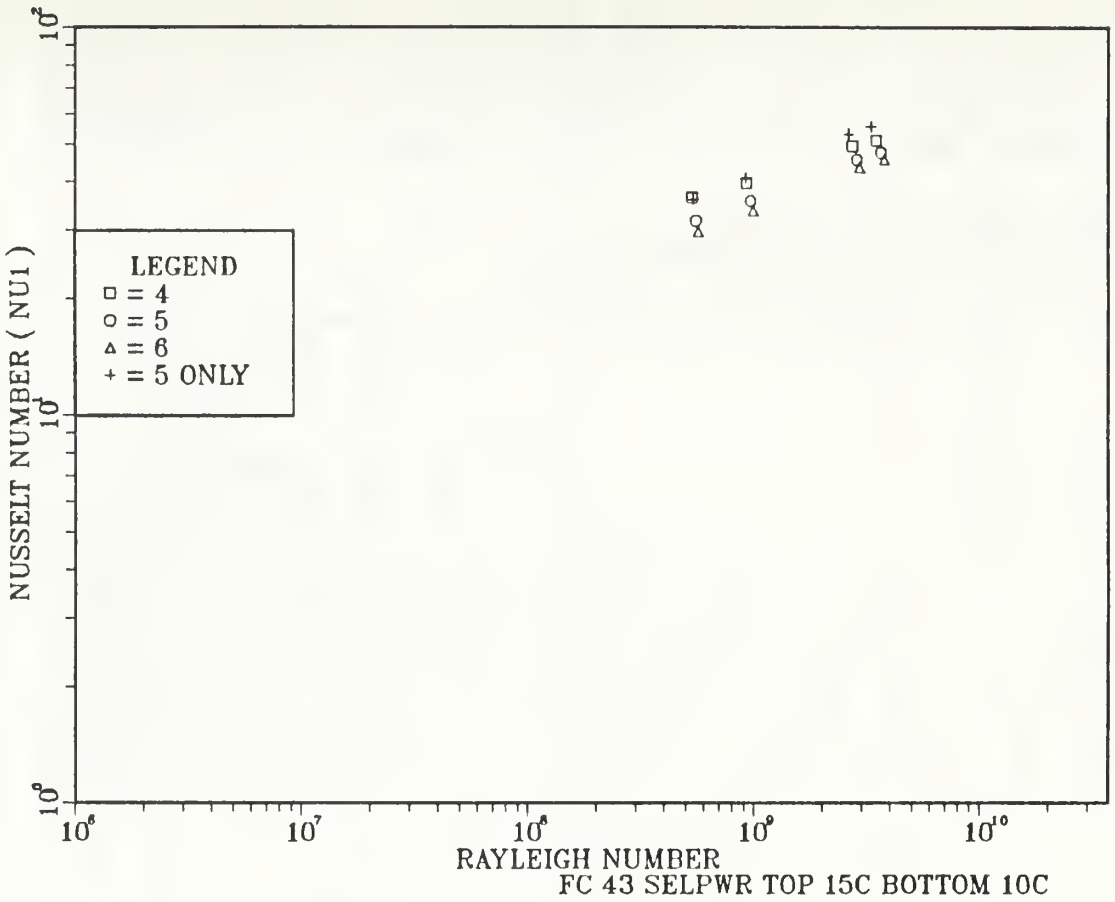

Figure 3.19 **Plot of Nusselt Number (Nu1) vs. Rayleigh Number (Ra_f) for Dielectric FC-43 during Selective Powering of Components using Standard Surface Boundary Conditions.**

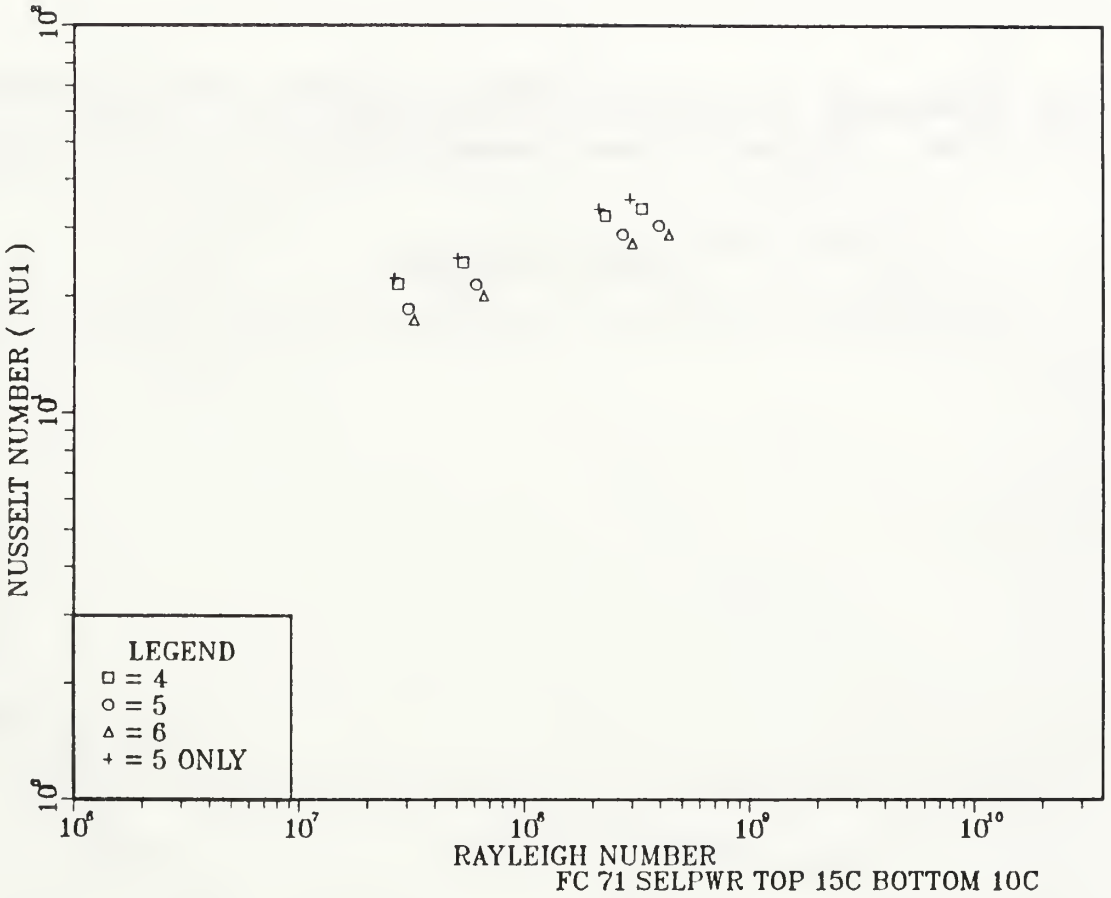

Figure 3.20 **Plot of Nusselt Number (Nu1) vs. Rayleigh Number (Ra_f) for Dielectric FC-71 during Selective Powering of Components using Standard Surface Boundary Conditions.**

B . FLOW VISUALIZATION

Flow visualization was conducted with the protrusion array oriented vertically with the chamber width of 30 mm. The chamber width was chosen to allow comparisons with the previous studies of Benedict [Ref. 17] and Torres [Ref. 18]. Visualizations were conducted in 3 vertical planes. As identified in Figure 3.21;

Plane 1 - aimed parallel towards the component through the sidewall

Plane 2 - aimed near and parallel to the front face of the enclosure through the sidewall

Plane 3 - Not shown in Figure 3.21, but was aimed perpendicular to the component and was viewed through the sidewall

A small amount of powered magnesium (325 Mesh) was introduced into the FC-75 Fluorinert dielectric fluid. These particles have a specific gravity of 1.92 gm/cm^3 and are almost neutrally buoyant in the Fluorinert fluids.

The top and bottom surfaces of the enclosure were maintained at uniform temperatures close to the ambient levels. Visualizations were performed for input power levels of 0.1, 0.7, and 1.5 W.

1. Flow Pattern with No Power Input

Visualization with no power was used to investigate the baseline Natural Convection flow due to the temperature differences between the various chamber surfaces. The flow in plane 1 (Figure 3.22) consisted of a dominant clockwise flow, with both sidewall boundaries showing steady downward flow towards a stable stratified region located at the base of the chamber.

Near the front face in plane 2 (Figure 3.23) circulating twin cells were observed. Each cell had a dominant flow toward their respective sidewall and down toward the stable stratified region at the chamber base.

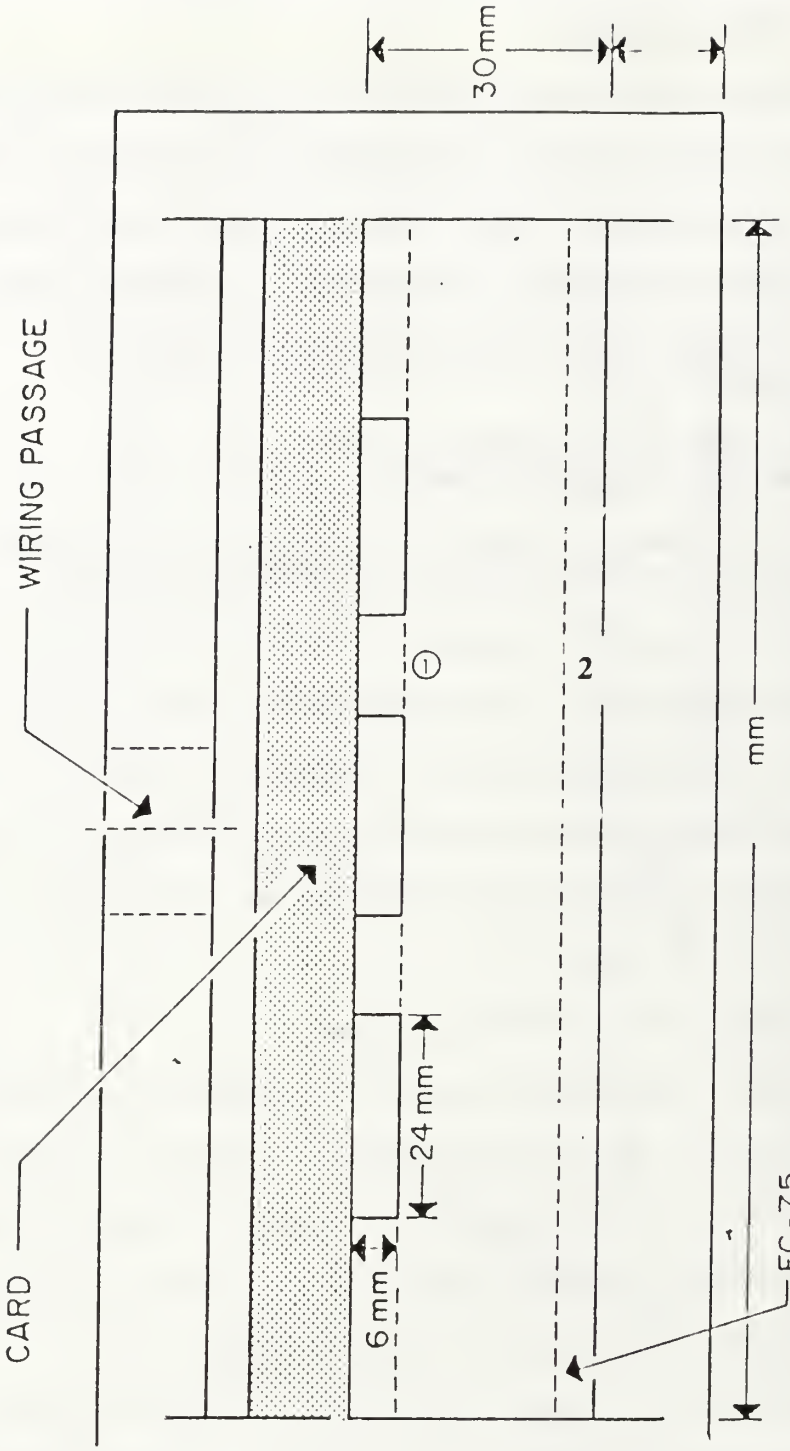

Figure 3.21 **Sidewall View of Enclosure with Substrate Located 30 mm from Front Face. Two Vertical Flow Planes are Identified with Respect to the Chamber.**

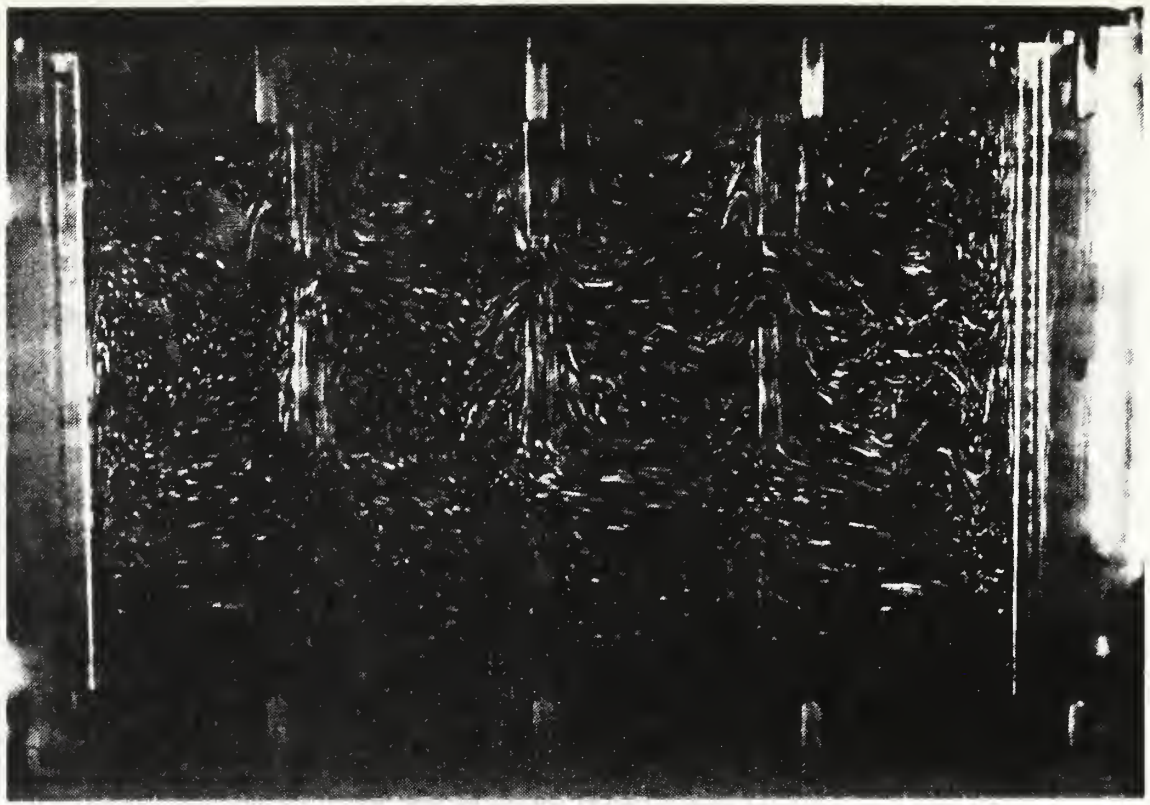

Figure 3.22 **Flow Visualization in Plane 1 with No Input Power (F4.0 for 15 Seconds).**

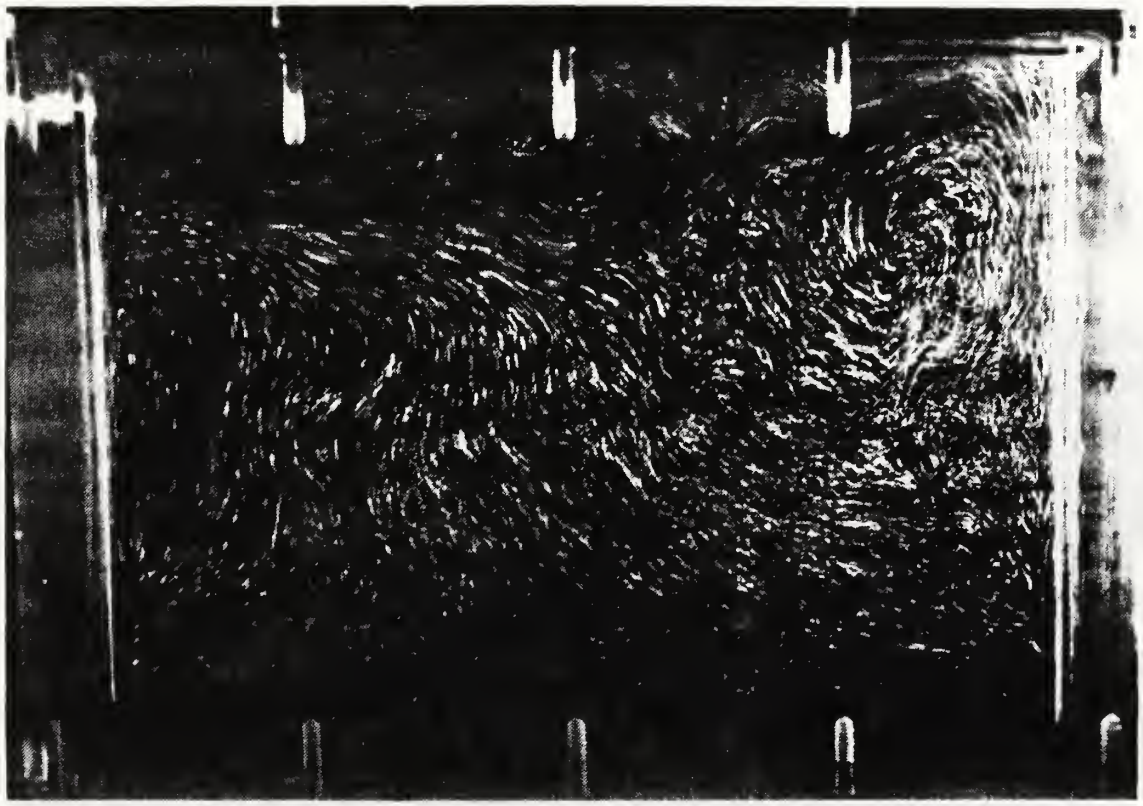

Figure 3.23 **Flow Visualization in Plane 2 with No Input Power (F2.8 for 15 Seconds).**

2. Flow Pattern at 0.1 W

With the heating of the components, a buoyant upflow was clearly evident in plane 1 (Figure 3.24). Once the flow reached the top of the chamber it was re-directed towards the sidewall boundaries and circulated back down into the stable stratified region of colder dielectric fluid at the enclosure bottom.

In plane 2 (Figure 3.25) the dual cell flow showed greater velocity along the sidewall boundaries, toward the stagnan region at the bottom of the enclosure.

3. Flow Pattern at 0.7 W.

Observations adjacent to the components in plane 1 (Figure 3.26) showed dominant upward flow only near the components. However small "eddies" were observed near many components. Also observed was the strong downward flow along the vertical sidewalls of the enclosure.

A strong clockwise circulation throughout the entire chamber was seen in plane 2 (Figure 3.27). The sidewall boundary layers were found to be similar to the previous power levels.

Looking at flow patterns in plane 3 (Figure 3.28), a 3 dimensional flow structure was evident with an upflow near the components, an outward flow along the enclosures' top boundary, and a downflow along the enclosure front face into the colder stably stratified region near the bottom.

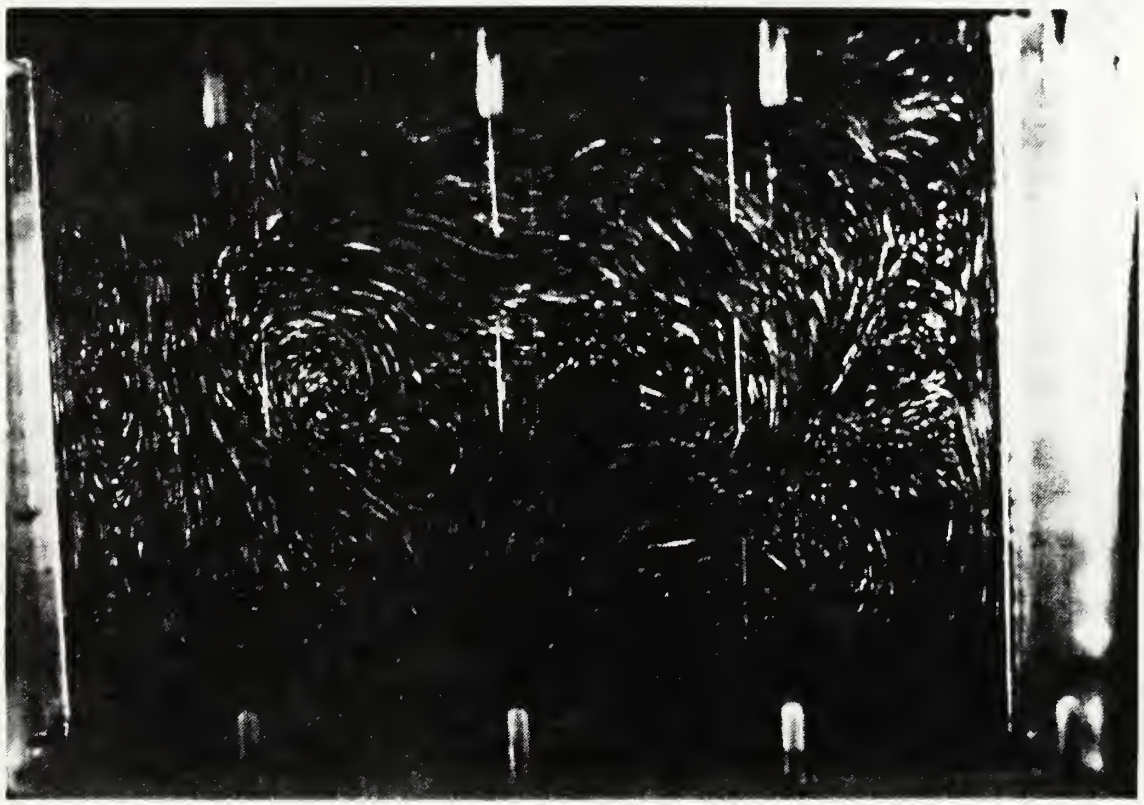

Figure 3.24 **Flow Visualization in Plane 1 with an Input Component Power of 0.1W (F4.0 for 15 Seconds).**

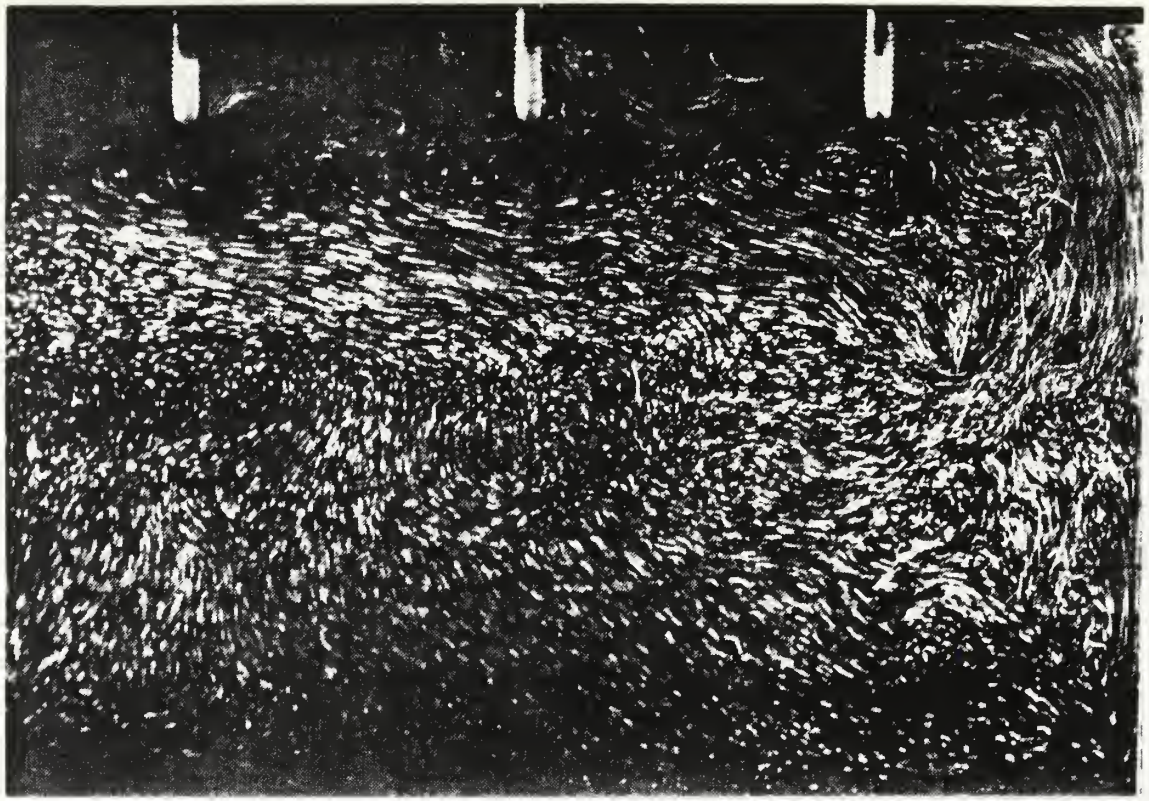

Figure 3.25 **Flow Visualization in Plane 2 with an Input Component Power of 0.1W (F4.0 for 20 Seconds).**

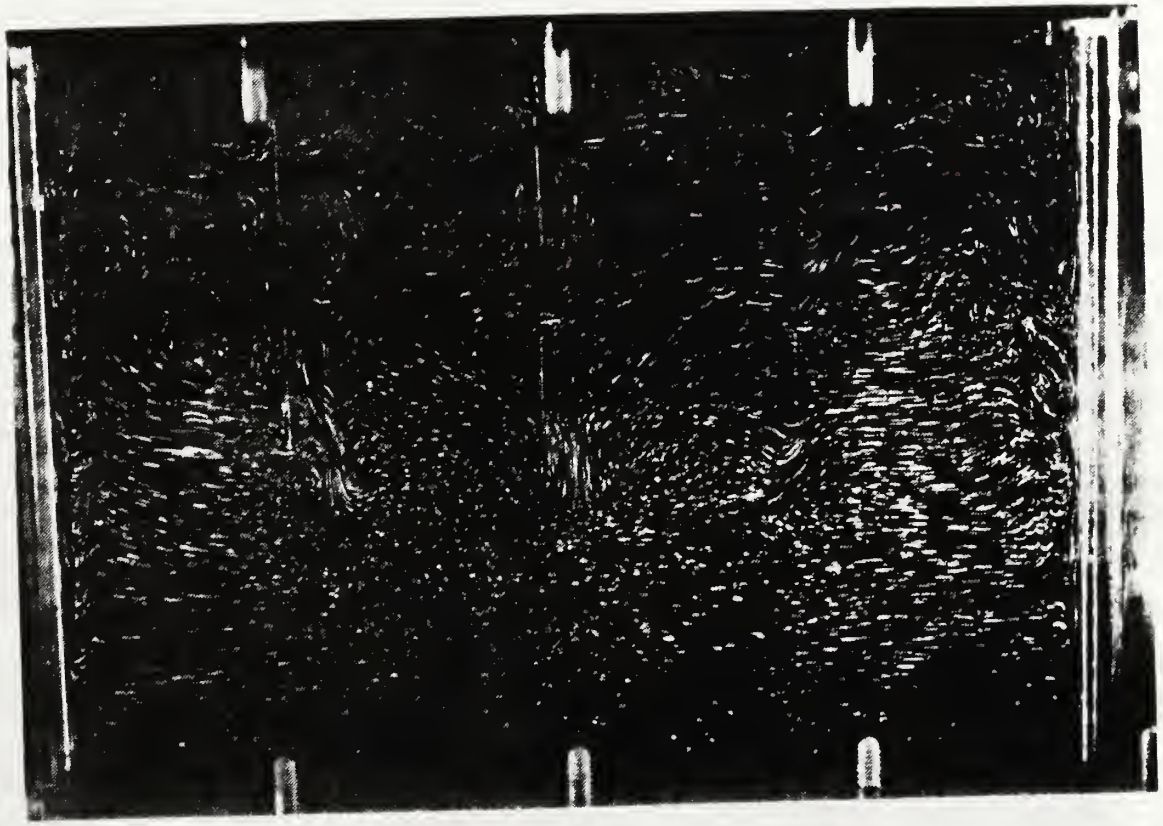

Figure 3.26 **Flow Visualization in Plane 1 with an Input Component Power of 0.7W (F2.8 for 15 Seconds).**

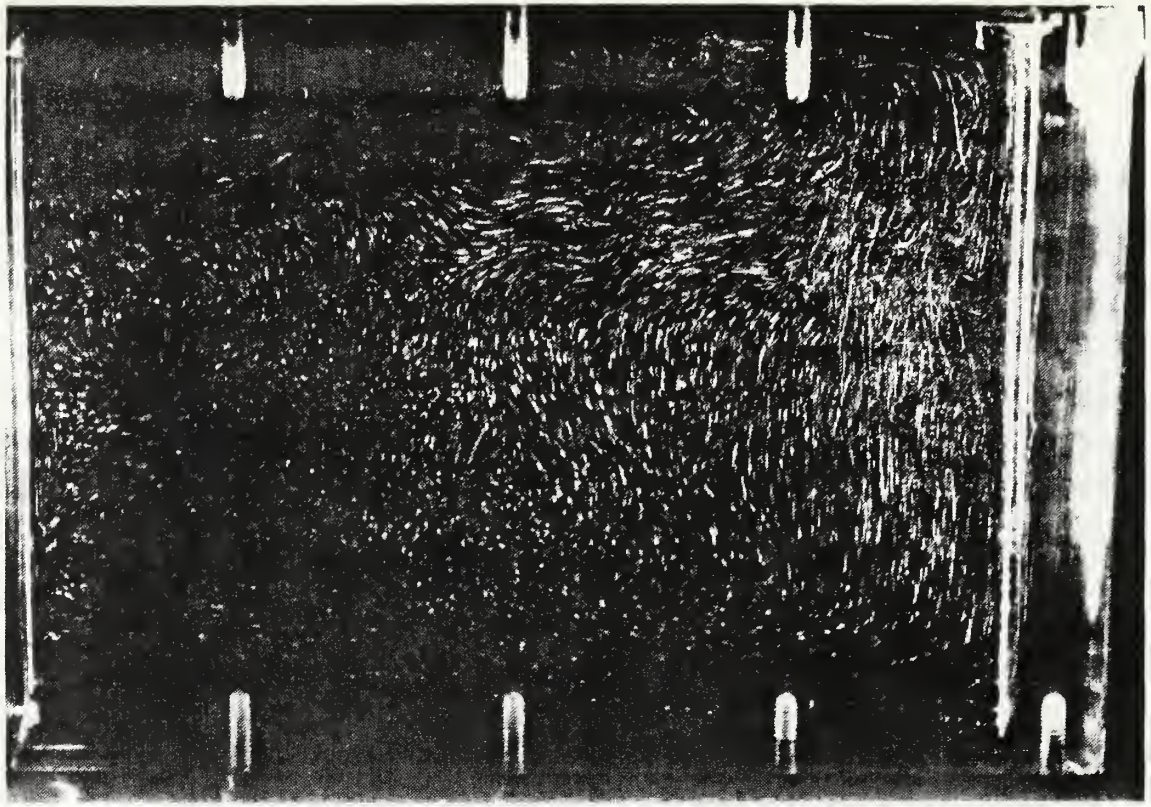

Figure 3.27 **Flow Visualization in Plane 2 with an Input Component Power of 0.7W (F2.8 for 10 Seconds).**

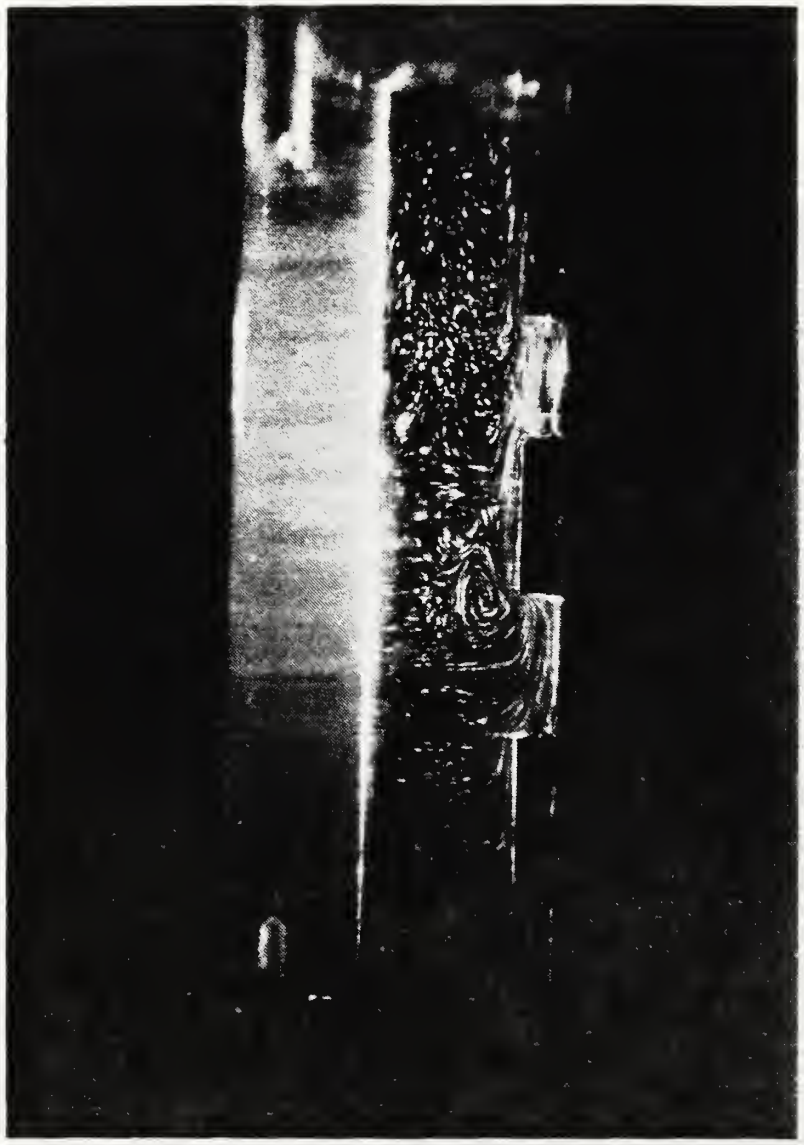

Figure 3.28 **Flow Visualization in Plane 3 with an Input Component Power of 0.7W (F2.8 for 15 Seconds).**

4. Flow Patterns at 1.5 W.

The flow observed at this power level appeared turbulent in nature. A pronounced upflow near the component columns observed in plane 1 (Figure 3.29) with formation of vortices at several locations. A dynamic downward flow along the enclosure sidewalls toward the bottom region was also found, as for the lower power levels.

In plane 2, upflow was also observed aligned with the component columns, which was not seen at the lower power levels. As seen in Figure 3.30, the presence of several small eddies were very evident. Observation of the 3 dimensional flow about plane 3 (Figures 3.31, 3.32, and 3.33), also indicates a localized buoyant upflow region near the components.

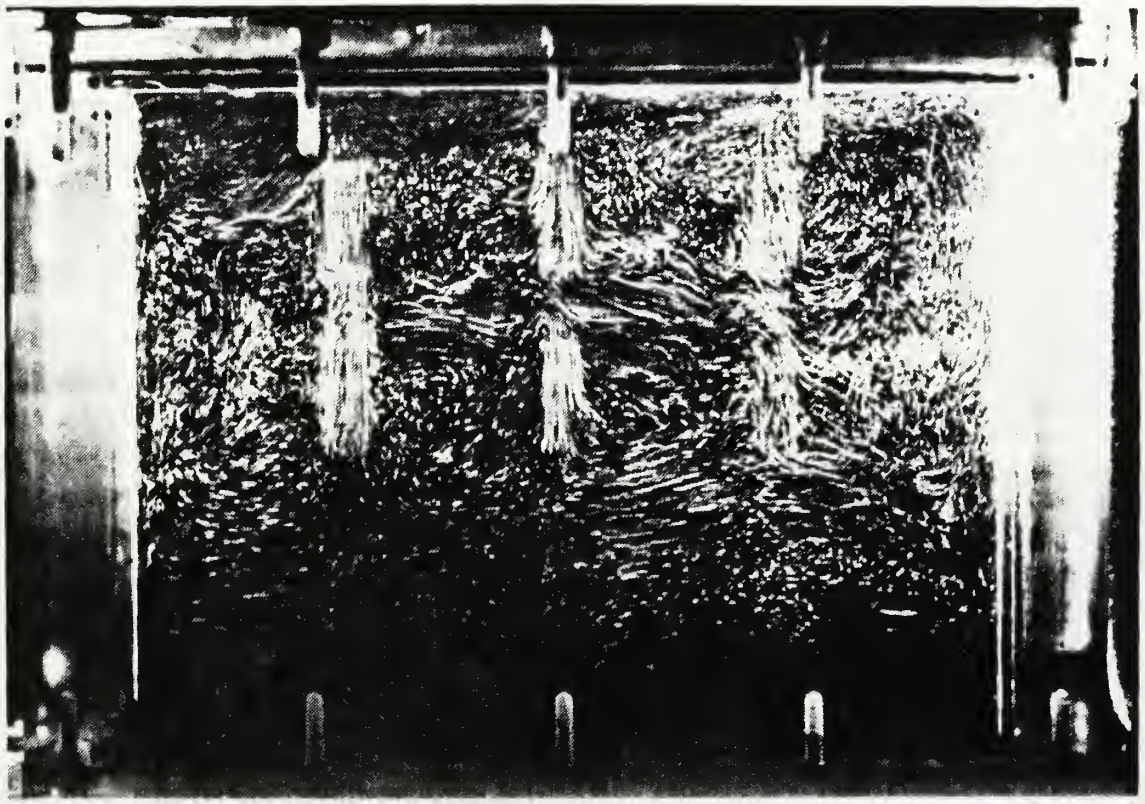

Figure 3.29 **Flow Visualization in Plane 1 with an Input Component Power of 1.5W (F2.8 for 10 Seconds).**

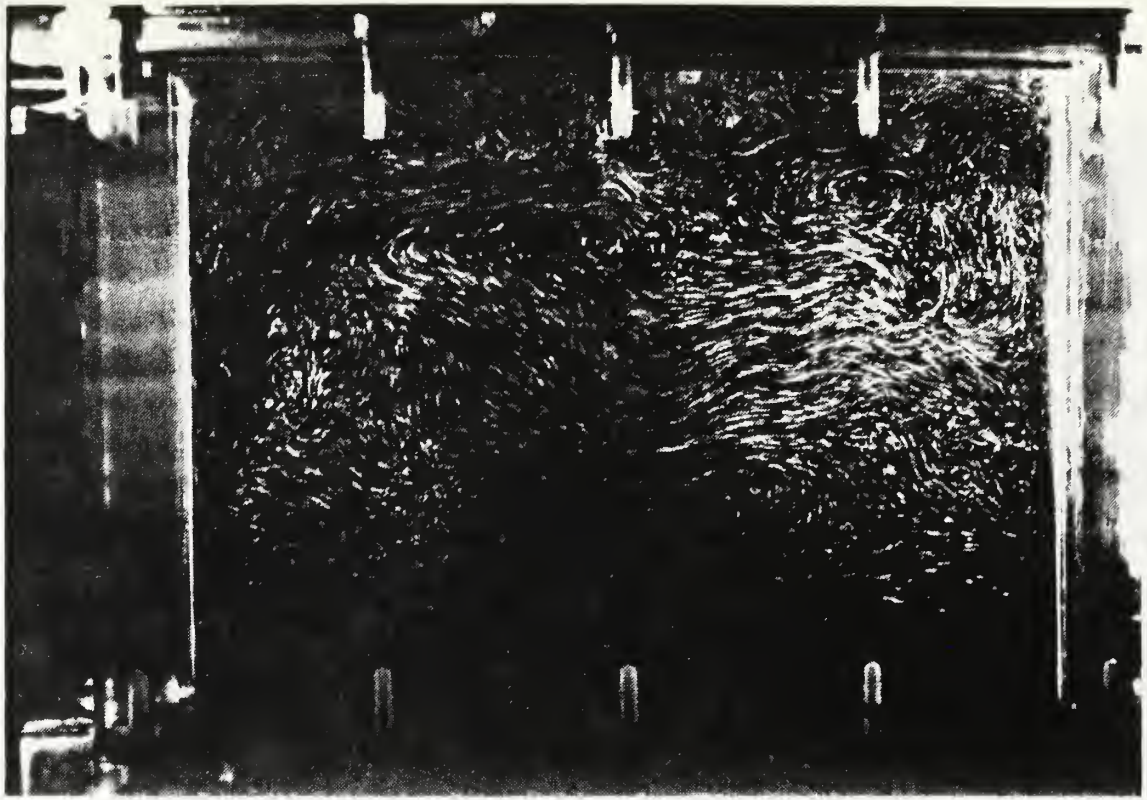

Figure 3.30 **Flow Visualization in Plane 2 with an Input Component Power of 1.5W (F2.8 for 10 Seconds).**

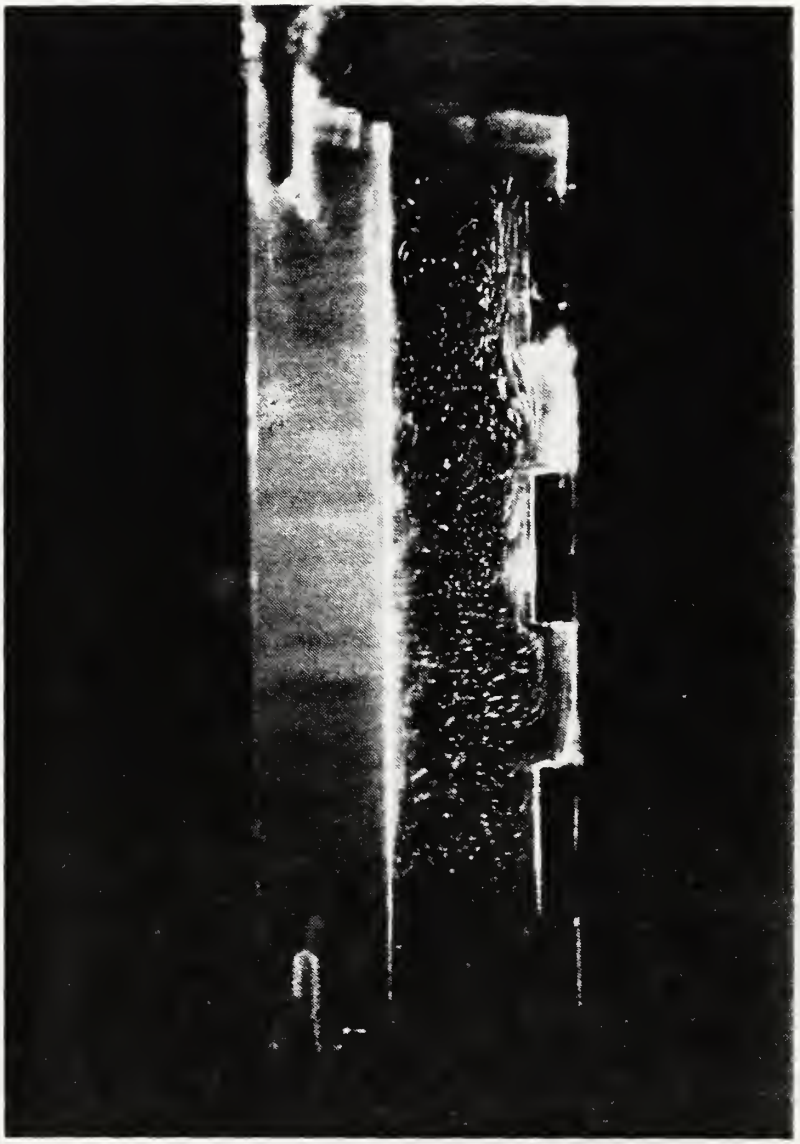

Figure 3.31 **Flow Visualization in Plane 3 with an Input Component Power of 1.5W (F2.8 for 10 Seconds).**

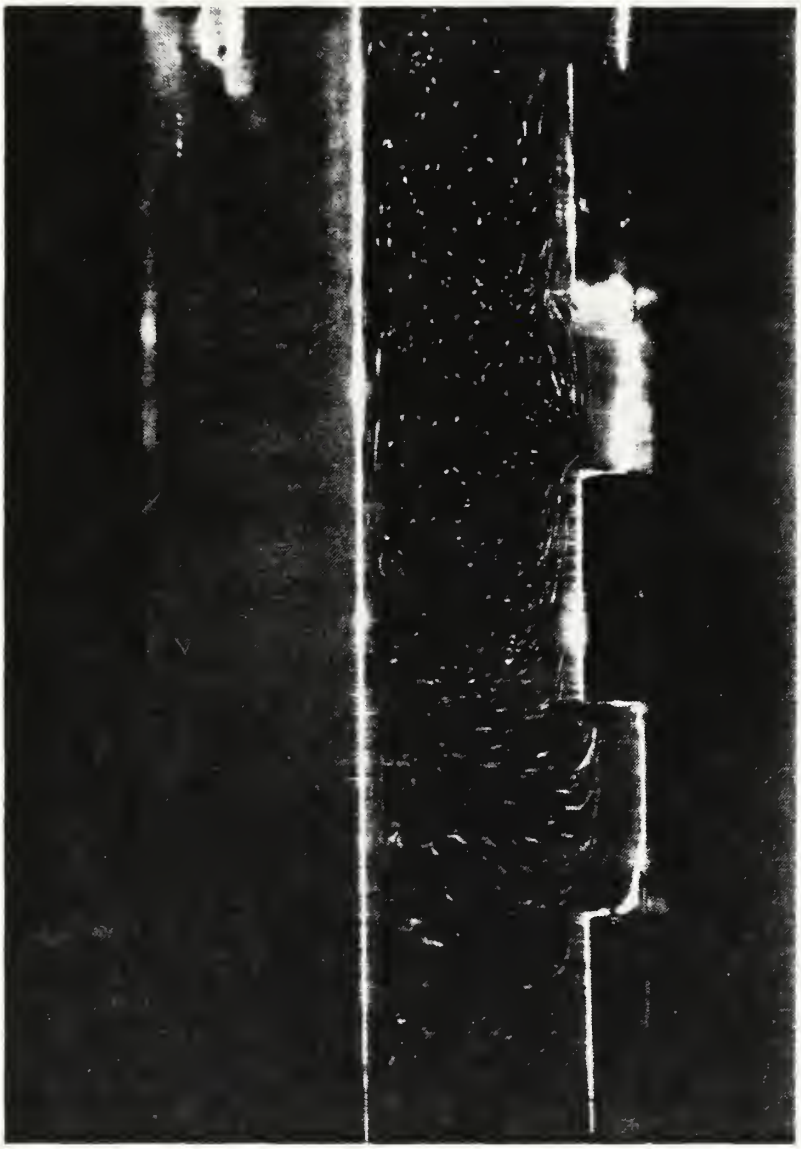

Figure 3.32 Close - Up Flow Visualization of Component 8 in Plane 3 with 1.5 W (F2.8 for 10 Seconds).

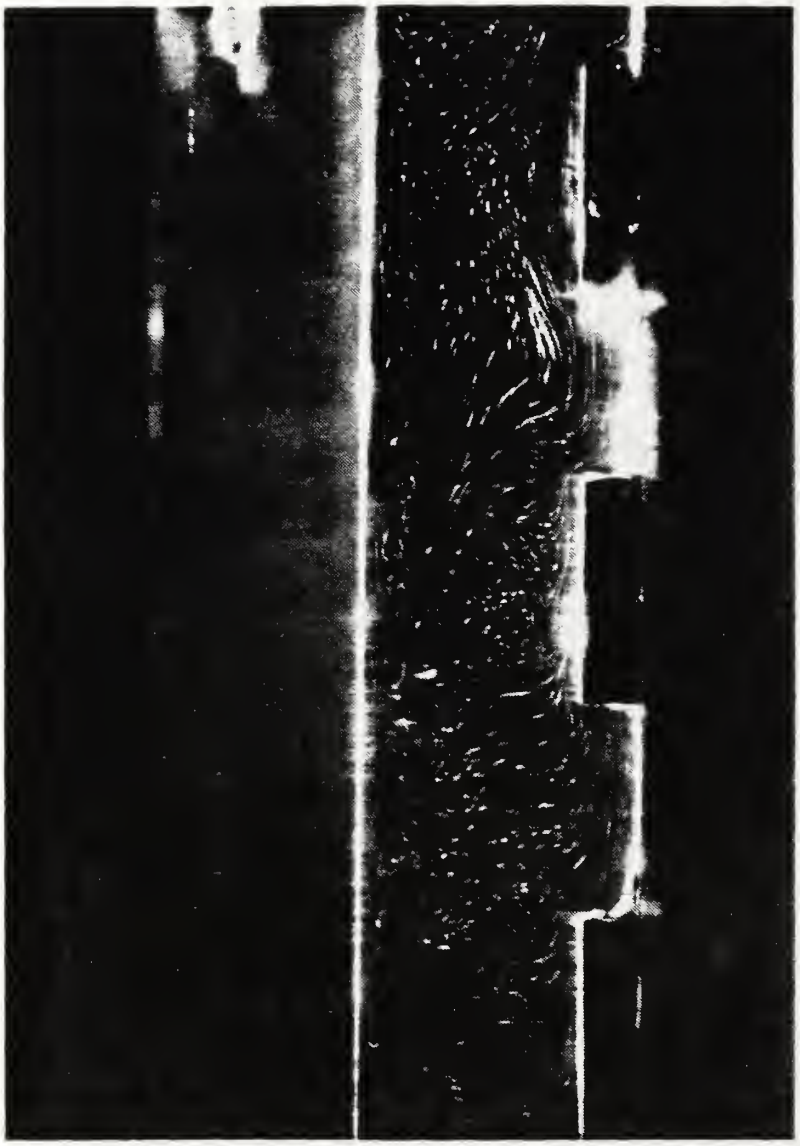

Figure 3.33 **Close - Up Flow Visualization of Component 8 in plane 3 with 1.5 W (F2.8 for 15 Seconds).**

IV. CONCLUSIONS

The thrust of this investigation was to increase the knowledge and data base concerning single - phase, direct liquid cooling of a small array of discrete protrusions. The data that was gathered established an understanding of the phenomena present for a 3 by 3 protrusion array for;

A. Flow Visualization

Primarily upflow very near Components, downflow along the boundaries.

B. Heat transfer Measurements

1). Effects of Prandtl number can be correlated by suitable non-dimensional parameters.

2). Enclosure Boundary Conditions relatively insignificant at higher power levels.

3). Component Orientation relatively unimportant.

4). Chamber Width decrease marginally degrades heat transfer.

5). Selective Powering results in higher Nusselt number compared to fully powered array at the same per component power.

V. RECOMMENDATIONS

1). Continuation of this investigation using other dielectric fluids with superior thermophysical properties .

2). Conduct detailed Flow Visualization investigations at several chamber widths.

3). Develop comprehensive 3 Dimensional numerical models of flow and heat transfer characteristics.

4). Manufacture a similar array with discrete flush heat sources, and conduct a thorough investigation using the same parameters and compare results with this study.

APPENDIX A SAMPLE CALCULATIONS

A. THERMOCOUPLE CONVERSION FROM VOLTAGES (emf) TO TEMPERATURES (° C)

HP 3497 Data Acquisition System (Channels 0 to 60 and 71 to 76) records given emf voltage readings in millivolts (mV) and convert to temperatures (° C). The coefficients are specifically for Omega Copper Constantan thermocouples.

$$T\ (°C) = 0.10086091 + (25727.9 * emf) - (767345.8 * emf^2) +$$

$$(7802.5596 * emf^3) - (9247486589.6 * emf^4) +$$

$$(6.98E11 * emf^5) - (2.66E13 * emf^6) + (3.94E14 * emf^7)$$

calculation: Using thermocouple 60 with FC-75 dielectric fluid at 1.5 Watt power level yields,

$emf = 0.000756\ V = 0.756\ mV$

$T = 20.70\ °C$

B. HEATER POWER (INPUT) CALCULATION

Hp 3497 Data Acquisition System (Channels 62 to 70) are used to measure individual heater component voltages.

$$Q_{in}\ (Watt) = (V_{in} - V_h) * V_h / R_p$$

where

$V_{in} \equiv$ Supply Voltage (Channel 61)

$V_h \equiv$ Voltage across Heaters

$R_p \equiv$ Precision Resistor

calculation: The power dissipation of heater number 5 with dielectric fluid FC-75 at 3.0 Watt power level was calculated to be

$$Q_{in} = 5.314 * (6.717 - 5.314) / 2.50$$

$$Q_{in} = 2.98 \text{ Watt}$$

C. AVERAGE TEMPERATURE CALCULATIONS

1. Average Component Temperature

The facial temperatures of the fluid exposed faces were first multiplied by their respective Areas, and then summed together. This result was then divided by the total fluid exposed Surface Area.

$$T_{avg} (°C) = \Sigma T_i * A_i / A_{total}$$

$$= [T(1) * A_{cen} + T(2) * A_{top} + T(3) * A_{right} +$$

$$T(4) * A_{left} + T(5) * A_{bot}] / A_{total}$$

where

$$A_{cen} = 0.024 * 0.008 = 1.92E\text{-}4 \text{ m}^2$$

$$A_{top} = A_{bot} = 0.006 * 0.008 = 4.85E\text{-}5 \text{ m}^2$$

$$A_{right} = A_{left} = 0.006 * 0.024 = 1.44E\text{-}4 \text{ m}^2$$

$$A_{total} = \Sigma A_i = 5.76E\text{-}4 \text{ m}^2$$

calculation: Using component 5 at the 3.0 W power level yields

$$T_{avg} (°C) = [(54.10 * 1.92E\text{-}4) + (54.93 * 4.8E\text{-}5) + (54.01 *$$

$$1.44E\text{-}4) + (54.42 * 1.44E\text{-}4) + (51.80 * 4.8E\text{-}5)] / 5.76E\text{-}4$$

$$T_{avg} = 54.04 °C$$

2. Average Sink Temperature

Heat Exchanger Channels are averaged together.

$$T_{sink}\,(^{\circ}C) = \Sigma\,[T_{top} + T_{bot}\,] / \text{Number of Thermocouples}$$

calculation: Using the 3.0 W power level

$$T_{sink}\,(^{\circ}C) = [10.123 + 10.098 + 9.947 + 14.879 + 14.929] / 5$$

$$T_{sink} = 11.99\ ^{\circ}C$$

3. Average Film Temperature

Fluid film temperature is approximated as:

$$T_{film}\,(^{\circ}C) = [\,T_{avg} + T_{sink}\,] / 2$$

calculation: Using the previously determined values yields,

$$T_{film}\,(^{\circ}C) = [\,54.04 + 11.99\,] / 2$$

$$T_{film} = 33.02\ ^{\circ}C$$

D. SUBSTRATE CONDUCTION LOSS CALCULATION

$$Q_{loss}\,(W) = \Delta T / R_c$$

where

$$R_c = L / k * A$$

$$= 0.0195\ m / (0.195\ W/m\ C)(0.008 * 0.024\ m^2)$$

$$= 520.83\ ^{\circ}C/W$$

where

L ≡ Plexiglass Substrate Thickness

k ≡ Thermal Conductivity of Plexiglass

A ≡ Back Area of Individual Component

calculation: Using the 3.0 W power level yields

$$Q_{loss}\,(W) = [\ 64.93 - 30.56\ ] / 520.83$$

$$Q_{loss} = 0.07\ W$$

E. CONVECTION COEFFICIENT DETERMINATION

Recall, Newton's Law of Cooling

$$Q_{net} = Q - Q_{loss} = h\,A_{total}\,\Delta T$$

Solving for h, yields

$$h\,(W / m^2\,C) = [\ Q - Q_{loss}\ ] / A_{total}\,(T_{avg} - T_{sink})$$

calculation: Using the 3.0 W power level

$$h\,(W/ m^2\,C) = [\ 3.0 - 0.07\ ] / 5.76E\text{-}4\ (\ 54.04 - 11.99\ )$$

$$h = [\ 2.93\ ] / 5.76E\text{-}4\ (\ 42.05\ )$$

$$h = 120.97\ W / m^2\,C$$

F. FLUID PROPERTIES DETERMINATION

1. Thermal Conductivity k [W / m °C]

From figure 5 of the 3M Corportation Flourinert Product Manual, the Thermal Conductivity coefficient curves have been determined to be:

FC - 75 $0.065 - 7.89474E\text{-}5 * T_{film}$

FC - 43 $0.06660 - 9.864E\text{-}6 * T_{film}$

FC - 71 0.071

calculation: Using FC-75 with power level 3.0 W yields

$$k_{fluid}\,(W / m\,C) = 0.065 - (\ 7.89474E\text{-}5 * 33.02\ )$$

$$k_{fluid} = 0.0624\ W / m\,C$$

2. Density ρ [**Kg / m³**]

Using the expression on Table 4B and constants presented in Table 4C of the Product Manual yields;

FC - 75 $(1.825 - 0.00246 * T_{film}) * 1000$

FC - 43 $(1.913 - 0.00218 * T_{film}) * 1000$

FC - 71 $(2.002 - 0.00224 * T_{film}) * 1000$

T_{film} temperatures must be in units of °C

calculation: Using FC-75 with the 3.0 W power level yields

$$\rho (Kg / m^3) = [1.825 - (0.00246 * 33.02)] * 1000$$

$$\rho = 1743.77 \ Kg / m^3$$

3. Kinematic Viscosity υ [**m ² / s**]

From figure 3 and determining a 4 th order curve fit yields:

FC - 75 $[1.4074 - 2.96E\text{-}2 * T_{film} + 3.8018E\text{-}4 * T_{film}^2$

$- 2.7308E\text{-}6 * T_{film}^3 + 8.1679E\text{-}9 * T_{film}^4] 1E\text{-}6$

FC - 43 $[8.8750 - 0.47007 * T_{film} + 1.3870E\text{-}2 * T_{film}^2$

$- 2.1469E\text{-}4 * T_{film}^3 + 1.3139E\text{-}6 * T_{film}^4] 1E\text{-}6$

FC - 71 $[251.62 - 13.723 * T_{film} + 0.30561 * T_{film}^2$

$- 3.1704E\text{-}3 * T_{film}^3 + 1.2668E\text{-}5 * T_{film}^4] 1E\text{-}6$

calculation: Using FC-75 case with 3.0 W power level yields

$$\upsilon\ (m^2/s) = [1.4074 - 2.96E\text{-}2\ (33.02) + 3.8018E\text{-}4\ (33.02)^2 - 2.7308E\text{-}6\ (33.02)^3 + 8.1679E\text{-}9\ (33.02)^4]\ 1E\text{-}6$$

$$\upsilon = 0.7546E\text{-}6\ m^2/s$$

4. Specific Heat c_p [J / Kg °C]

For all Flourinert Electrochemicals (figure 4):

$$c_p\ (J/Kg\ ^\circ C) = (0.241111 + 3.70374E\text{-}4 * T_{film}) * 4186$$

calculation: Using the 3.0 W power level

$$c_p\ (J/Kg\ ^\circ C) = (0.2533) * 4186$$

$$c_p = 1060.5\ J/Kg\ ^\circ C$$

5. Thermal Diffusivity α [m^2 / s]

Recall

$$\alpha = k / \rho\ c_p$$

calculation: Using the 3.0 W power level yields

$$\alpha\ (m^2/s) = 0.0624 / (1743.77 * 1060.5)$$

$$\alpha = 33.74E\text{-}9\ m^2/s$$

6. Thermal Expansion Coefficient β [1 / °C]

Using expression in Table 4B and the constants presented in Table 4 C yields:

FC - 75 $0.00246 / (1.825 - 0.00246 * T_{film})$

FC - 43 $0.00218 / (1.913 - 0.00218 * T_{film})$

FC - 71 $0.00224 / (2.002 - 0.00224 * T_{film})$

T_{film} temperatures must be in units of °C

calculation: Using FC-75 case with the 3.0 W power level yields

$$\beta\ (1/°C) = 0.00246 / (1.825 - 0.0812)$$

$$\beta = 0.001411 / °C$$

G. CHARACTERISTIC LENGTHS

Two Characteristic Lengths have been formulated to enable comparisions with other Experimental and Numerical Investigations.

L1 ≡ Vertical length (0.024 m)

L2 ≡ Sum of the Ratios of Area to Perimeter of the Fluid exposed faces.

$$L2 = \sum A(I)/P(I)$$
$$= [(0.024 * 0.008)/0.064] + 2 * [(0.008 * 0.006)/0.028] + 2 * [(0.024 * 0.006)/0.060]$$
$$= [0.003 + 2(0.00171429) + 2(0.0024)]\ m$$
$$L2 = 0.00112286\ m$$

H. NUSSELT NUMBER DETERMINATION

Recall,

$$Nu = h\ L / k$$

each of the characteristic lengths defined above as used. Therefore,

$$Nu1 = h\ L1 / k_{fluid}$$

$$Nu2 = h\ L2 / k_{fluid}$$

calculation: Using FC-75 and the vertical length, Nu1 was determined

$$Nu1 = 120.97 * 0.024 / 0.0624$$

$$Nu1 = 46.53$$

I. GRASHOF NUMBER DETERMINATION

The Grashof Number indicates the ratio of Buoyancy force to the Viscous force. Therefore,

$$Gr = g * \beta * L^3 * \Delta T / \upsilon^2$$

where,

$g \equiv$ Gravitational Constant

calculation: Using the 3.0 W power level yields

$$Gr = 9.81 * 0.001411 * (0.024)^3 * 42.05 / (0.7546E\text{-}6)^2$$

$$Gr = 8.046E\text{-}6 / 5.694E\text{-}13$$

$$Gr = 14.13E+6$$

J. PRANDTL NUMBER DETERMINATION

Recall,

$$Pr \equiv \upsilon / \alpha$$

calculation: Using the Fc-75 case with the 3.0 W power level

$$Pr = 0.7546E\text{-}6 / 33.74E\text{-}9$$

$$Pr = 22.37$$

K. TEMPERATURE BASED RAYLEIGH NUMBER DETERMINATION

Recall,

$$Ra_t \equiv Gr * Pr$$

$$= g * \beta * L^3 * \Delta T / \upsilon * \alpha$$

calculation: Using the 3.0 W power level yields

$$Ra_t = 9.81 * 0.001411 * (0.024)^3 * 42.05 / (0.7546E\text{-}6 * 33.74E\text{-}9)$$

$$Ra_t = 8.046E\text{-}6 / 25.46E\text{-}9 = 316.03E+6$$

L. FLUX BASED RAYLEIGH NUMBER

Recall,

$$Ra_f \equiv g * \beta * L^4 * Q_{net} / k * \alpha * \upsilon * A_{total}$$

calculation: Using the 3.0 W power level yields

$$Ra_f = [9.81 * 0.001411 * (0.024)^4 * 2.93] /$$

$$[0.0624 * 0.7546E\text{-}6 * 33.74E\text{-}9 * 5.76E\text{-}4]$$

$$Ra_f = 14.71E+9$$

APPENDIX B

UNCERTAINTY ANALYSIS

A. UNCERTAINTIES IN NET POWER ADDED INTO THE FLUID

Recall,

$$Q_{net} = Q_{in} - Q_{loss}$$

1. Q_{in} [Watt]

Input Power is a function of the individual heater voltage , the input voltage, and the precision resistors. Therefore,

$$\partial Q_{in} / \partial V_h = Volt - 2 * V_h / R_p$$

$$\partial Q_{in} / \partial Volt = V_h / R_p$$

$$\partial Q_{in} / \partial R_p = - V_h [Volt - V_h] / R_p$$

Thus,

$$U_{Qin} = [(\partial Q_{in} / \partial V_h)^2 * U_{Vh}^2 + (\partial Q_{in} / \partial Volt)^2 * U_{Volt}^2 + (\partial Q_{in} / \partial R_p)^2 * U_{Rp}^2]^{1/2}$$

where,

$U_{Vh} = \pm$ 0.001 Volt Resolution / Precision of Measuring Device

$U_{Volt} = \pm$ 0.001 Volt

$U_{Rp} = \pm$ 0.05 Ω

calculation: Using FC-75 dielectric fluid with Chip 5 on the 3.0 W power level yields,

$V_h = 5.314$ V

Volt = 6.717 V

$R_p = 2.50\ \Omega$

Therefore,

$$\partial Q_{in} / \partial V_h = [\ 6.717 - (\ 2 * 5.314\ )] / 2.50 = -\ 1.5644$$

$$\partial Q_{in} / \partial \text{Volt} = 5.314 / 2.50 = 2.1256$$

$$\partial Q_{in} / \partial R_p = [-5.314 * (\ 6.717 - 5.314\ )] / 2.50 = -2.982$$

Thus

$$U_{Qin} = [\ (\ 1.5644)^2\ (0.001)^2 + (2.1256)^2 (0.001)^2 + (2.982)^2 (0.05)^2\ ]^{1/2}$$

$$U_{Qin} = 0.1491$$

Percentage error was derived by:

$$U_{Qin} / Q_{in} = [0.1491 / 2.98\ ] * 100\% = 5.00\ \%$$

$Q_{in} = 2.98 \pm 5.0\%$ Watt

2. Q_{loss} [Watt]

Recall,

$$Q_{loss} = \Delta T / R_c$$

The Energy loss due to conduction is a function of the change in temperature, and the total thermal resistance. Therefore,

$$\partial Q_{loss} / \partial \Delta T = 1 / R_c$$

$$\partial Q_{loss} / \partial R_c = \Delta T / R_c^2$$

Thus,

$$U_{Qloss} = [(1 / R_c) ^2 * U_{\Delta T}^2 + (- \Delta T / R_c^2) ^2 * U_{Rc}^2] ^{1/}$$

where,

$U_{\Delta T} = 10\%$

$U_{Rc} = 10\%$

calculation: Using FC-75 case with the 3.0 W power level yields

$R_c = 520.97 * 10\% = 52.097$

$\Delta T = 64.93 - 30.56 = 34.37$ °C

Therefore,

$\partial Q_{loss} / \partial R_c = 1 / 520.97 = 0.001919$

$\partial Q_{loss} / \partial \Delta T = 34.37 / (520.97)^2 = 126.64E-6$

Thus,

$U_{Qloss} = [(0.001919)^2 (3.437)^2 +(126.64E-6)^2 (52.097)^2]^{1/2}$

$U_{Qloss} = 0.00933$

Pecentage error was derived by:

$U_{Qloss} / Q_{loss} = 0.00933 / 0.07 * 100\% = 13.3\%$

$\underline{Q_{loss} = 0.07 \pm 13.3\% \text{ Watt}}$

3. Q_{net} [Watt]

Combining the results of the power and energy loss uncertainties yields the final uncertainty calculation for Q_{net}:

$$U_{Qnet} = [(U_{Qin})^2 + (U_{Qloss})^2]^{1/2}$$

calculation: Using FC-75 with the 3.0 W power level yields,

$$U_{Qnet} = [(0.1491)^2 + (0.00933)^2]^{1/2}$$

$$U_{Qnet} = 0.1494$$

Percentage error was dervived by:

$$U_{Qnet} / Q_{net} = [0.1494 / 2.93] * 100\% = 5.10\%$$

$\underline{Q_{net} = 2.93 \pm 5.1\% \text{ Watt}}$

B. UNCERTAINTY IN NUSSELT NUMBER

Recall,

$$Q_{net} = h\ A_{total}\ (T_{avg} - T_{sink})$$

Solving for the Heat Transfer coefficient , h , yields,

$$h = Q_{net} / A_{total}\ (T_{avg} - T_{sink})$$

where the Heat Transfer coefficient is a function of the net power dissipated by the heater, total area, and the change in temperature. Therefore,

$$\partial h / \partial Q_{net} = 1 / A_{total}\, \Delta T$$

$$\partial h / \partial A_{total} = Q_{net} / A_{total}\, \Delta T$$

$$\partial h / \partial(\Delta T) = Q_{net} / A_{total}\, (\Delta T)^2$$

Thus,

$$U_h = [(\partial h / \partial Q_{net})^2 * U_{Qnet}^2 + (\partial h / \partial A_{total})^2 * U_{Atotal}$$

$$+ (\partial h / \partial \Delta T)^2 * U_{\Delta T}^2]^{1/2}$$

where,

$$U_{Atotal} = [(\partial A_{total}/\partial L)^2 * U_L^2 + (\partial A_{total}/\partial W)^2 * U_W^2 + (A_{total}/\partial H)^2 * U_H^2]^{1/2}$$

$$= [(2H + W)^2 (1E\text{-}4)^2 + 2 (L + W)^2 (1E\text{-}4)^2 +$$

$$(2H + L)^2 (1E\text{-}4)^2]^{1/2}$$

U_L = 1E-4 m

U_{Atotal} = 8.736E-6 m^2

$U_{\Delta T}$ = ± 1 %

calculation: Using Fc-75 at the 3.0 W power level yields,

ΔT = 54.04 - 11.99 = 42.05 °C

A_{total} = 5.76 E-4 m^2

Therefore,

$\partial h / \partial Q_{net}$ = 1 / [(42.05)(5.76E-4)] = 41.29

$\partial h / \partial A_{total}$ = 2.93 / [(42.05)(5.76E-4)] = 120.97

$\partial h / \partial(\Delta T)$ = 2.93 / [(5.76E-4)$(42.05)^2$] = 2.877

Thus,

$$U_h = [(41.29)^2 (0.1494)^2 + (120.97)^2 (8.736E\text{-}6)^2 +$$

$$(2.877)^2 (0.4205)^2]^{1/2}$$

U_h = 6.286

Percentage error was derived by:

U_h / h = [6.286 / 120.97] * 100% = 5.20 %

<u>h = 120.97 ± 5.2 %</u>

Recall, to determine the Nusselt Number

$$Nu = h L / k$$

The Nusselt Number is a function of the Heat Transfer Coefficient, Characteristic length, and the Thermal Conductivity. Therefore,

$$\partial Nu / \partial h = L / k_{fluid}$$

$$\partial Nu / \partial L = h / k_{fluid}$$

$$\partial Nu / \partial k = - h L / k_{fluid}^2$$

Thus,

$$U_{Nu} = [(\partial Nu / \partial h)^2 * U_h^2 + (\partial Nu / \partial L)^2 * U_L^2]^{1/2}$$

Assuming that the Dielectric Flourinert Fluids' properties are considered to have no uncertainty in this determination.

calculation: Using FC-75 with the 3.0 W power level yields,

$$\partial Nu1 / \partial h = 0.024 / 0.0624 = 0.3846$$

$$\partial Nu1 / \partial L = 120.97 / 0.0624 = 1938.6$$

Thus,

$$U_{Nu1} = [(0.3846)^2 (6.286)^2 + (1938.6)^2 (1E-4)^2]^{1/2}$$

$$U_{Nu1} = 2.425$$

Percentage error was derived by:

$$U_{Nu1} / Nu = [2.425 / 46.53] * 100\% = 5.2 \%$$

<u>Nu1 = 46.53 ± 5.2 %</u>

C. FLUX BASED RAYLEIGH NUMBER DETERMINATION

Recall the expression for the Rayleigh Number,

$$Ra_f = Gr_f \, Pr$$

where,

$$Gr_f = g \, \beta \, L^4 \, Q_{net} / k_f \, \upsilon^2 \, A_{total}$$

$$Pr = \upsilon / \alpha$$

The Grashof number is a function of gravity (g), volumetric expansion coefficient (β), characteristic length (L), net power dissipated (Q_{net}), thermal conductivity (k), kinematic viscosity (υ), and total wetted area (A_{total}). Therefore,

$$U_{Grf} / Gr_f = [(\partial Q_{net} / Q_{net})^2 + (4\partial L / L)^2 + (\partial A_{total} / A_{total})^2]^{1/2}$$

calculation: Using FC-75 at the 3.0 W power level yields

$$U_{Gr}/Gr_f = [(0.1494/2.93)^2 + (4E\text{-}4/0.024)^2 + (8.736E\text{-}6/5.76E\text{-}4)]^{1/2}$$

Percentage error was derived by:

$$U_{Grf} / Gr_f = U_{Raf} / Ra_f = 0.0558 * 100\% = 5.58\ \%$$

$\underline{Ra_f = 14.71\ E+9 \pm 5.58\ \%}$

APPENDIX C

The following graphical representations are for the sake of brevity to show the Heat Transfer measurements per component that was gathered during this investigation.

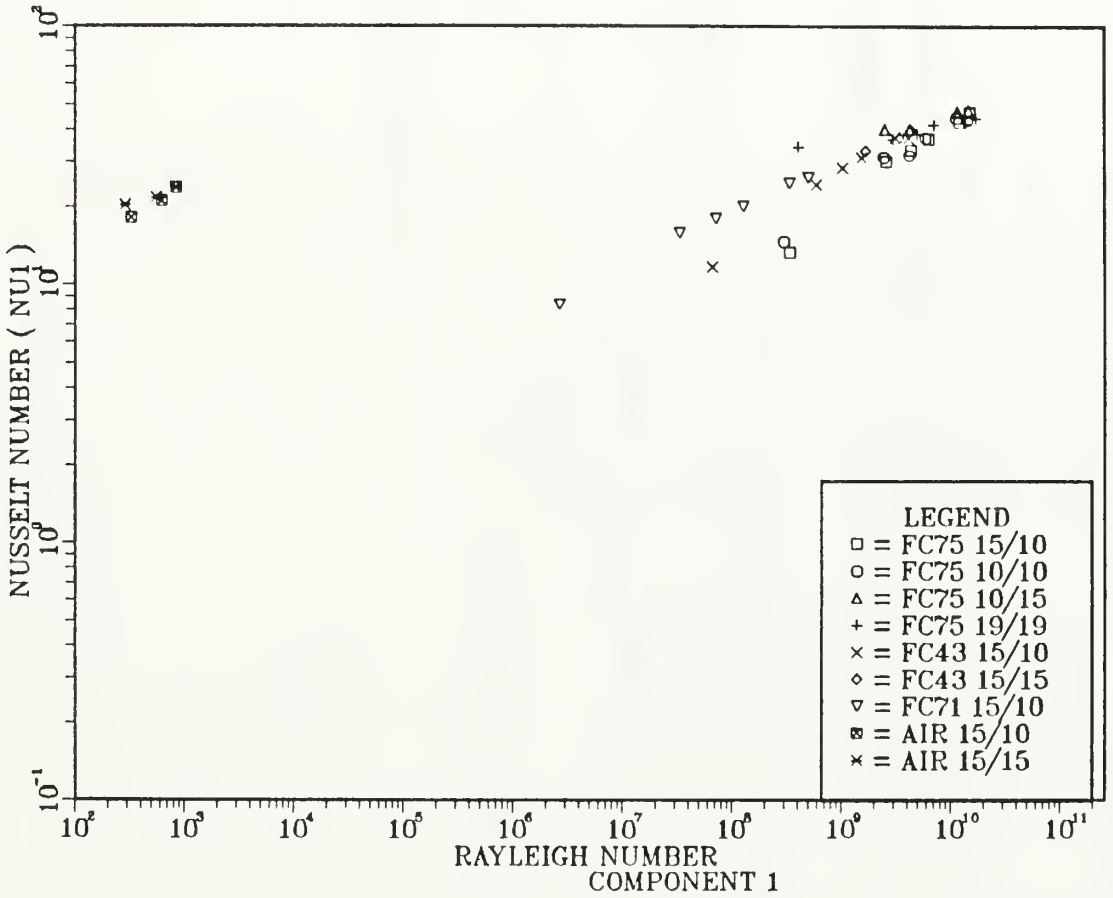

Figure C.1 **Plot of Nusselt Number (Nu1) vs. Rayleigh Number (Ra_f) for All Data Collected for Component 1.**

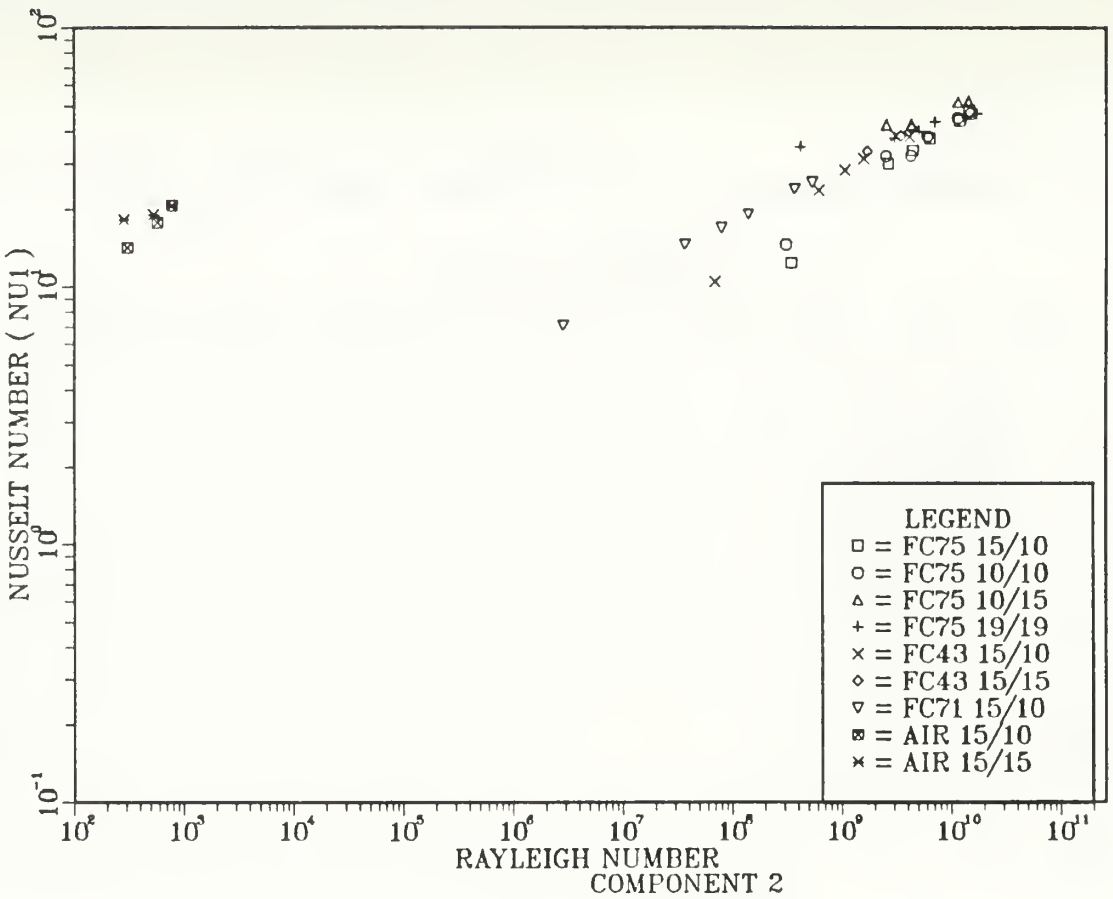

Figure C.2 **Plot of Nusselt Number (Nu1) vs. Rayleigh Number (Ra_f) for All Data Collected for Component 2.**

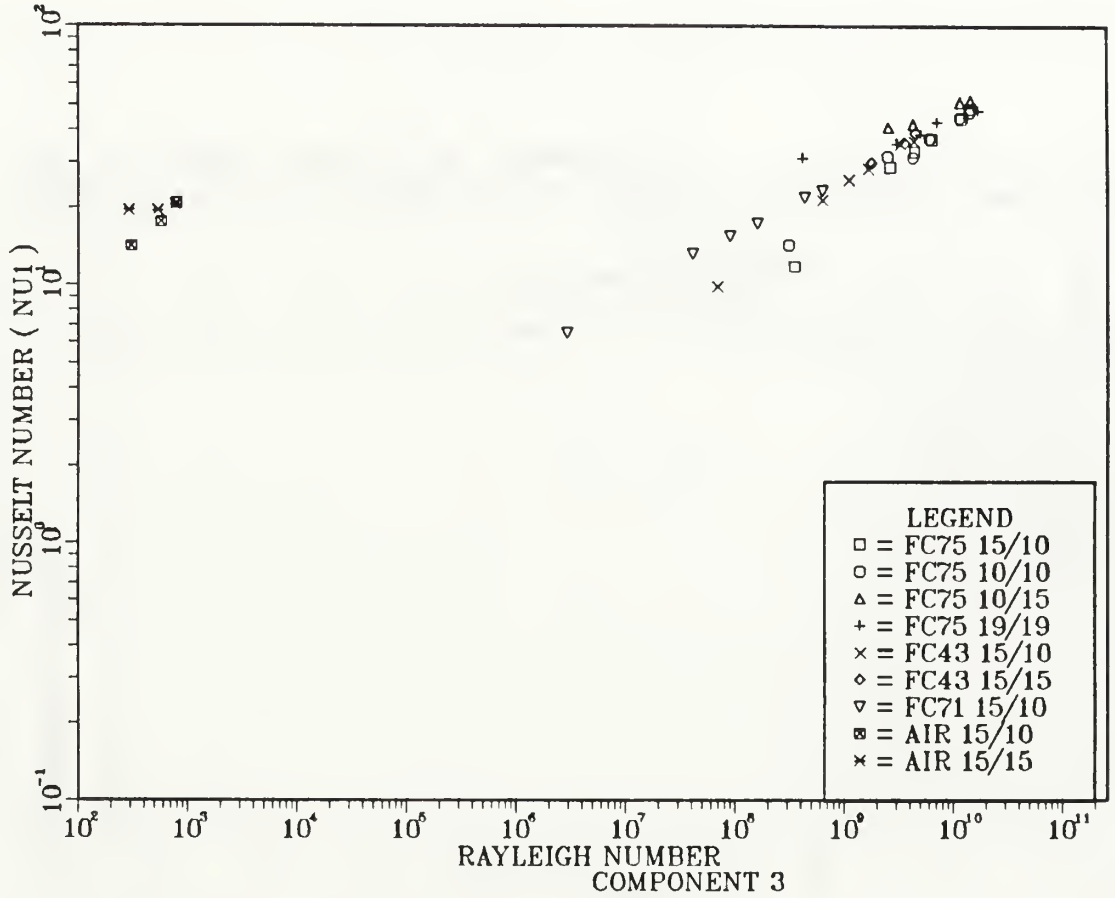

Figure C.3 **Plot of Nusselt Number (Nu1) vs. Rayleigh Number (Ra_f) for All Data Collected for Component 3.**

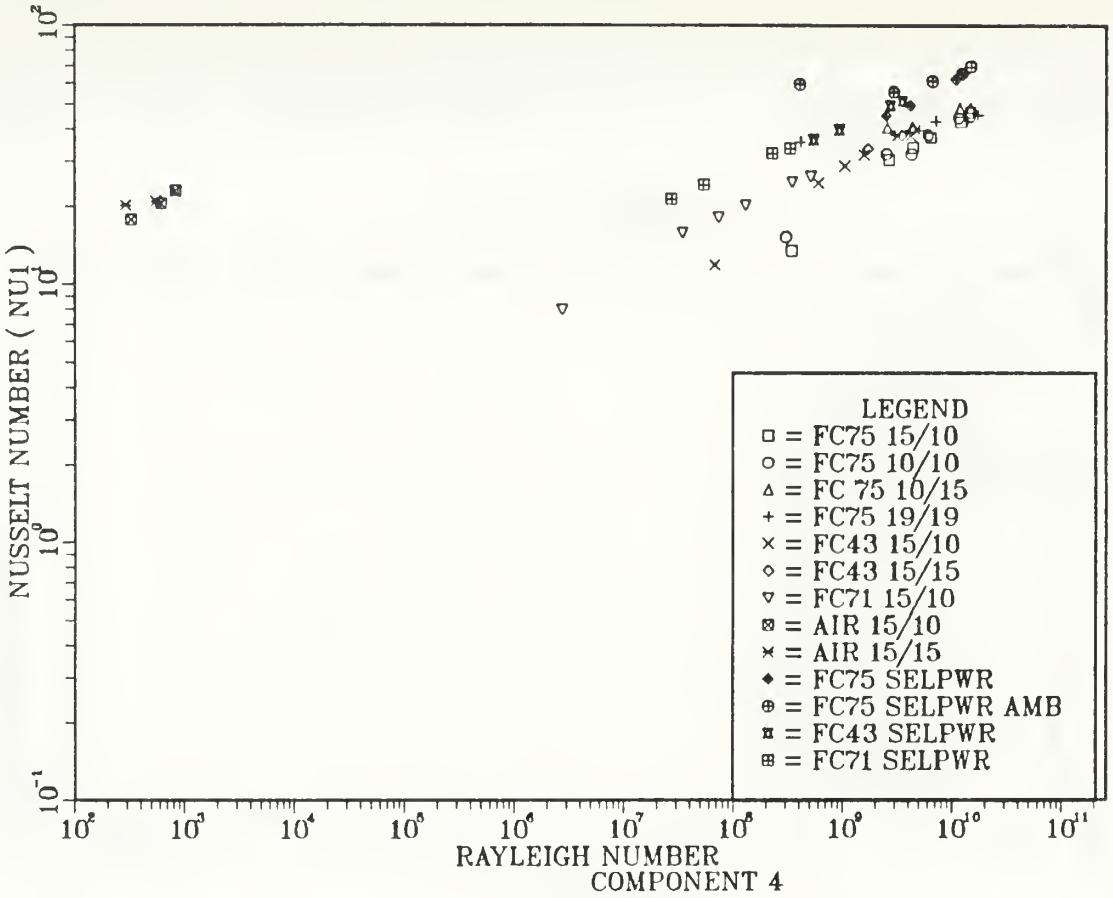

Figure C.4 **Plot of Nusselt Number (Nu1) vs. Rayleigh Number (Ra_f) for All Data Collected for Component 4.**

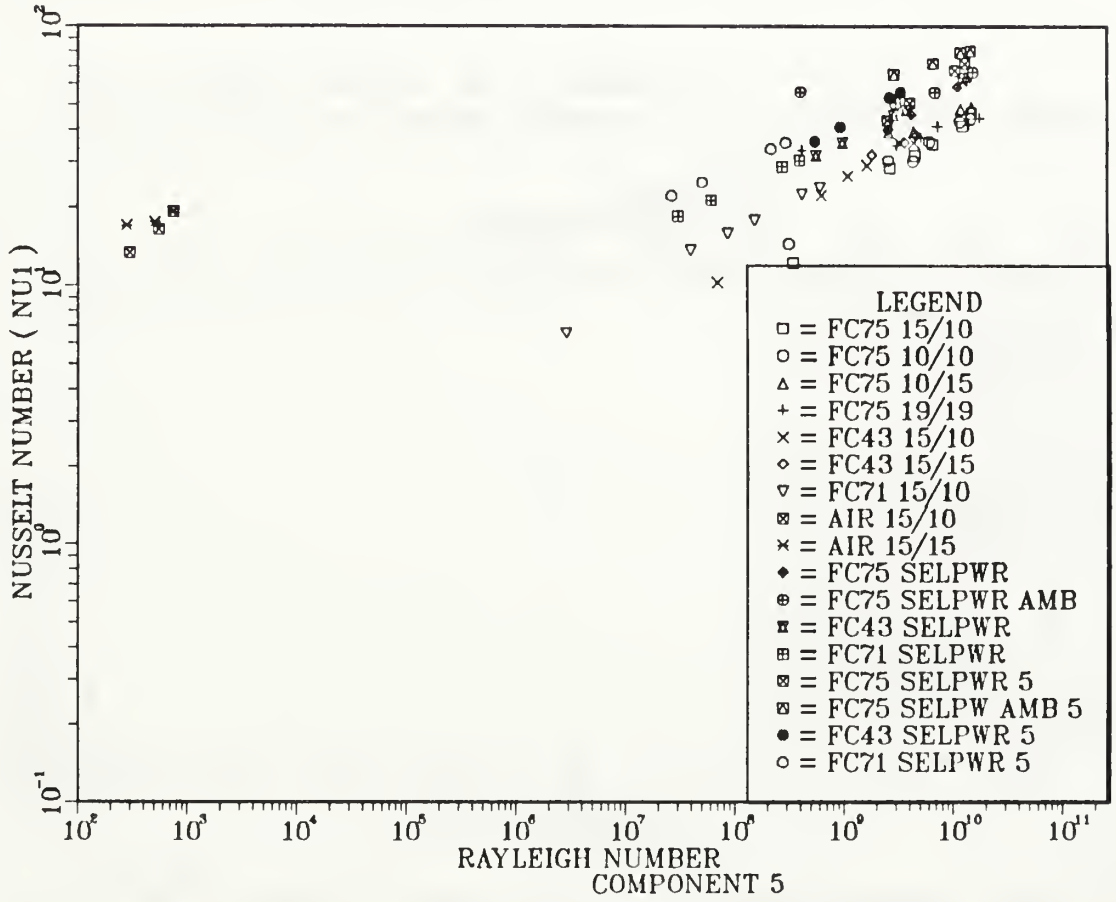

Figure C.5 Plot of Nusselt Number (Nu1) vs. Rayleigh Number (Ra_f) for All Data Collected for Component 5.

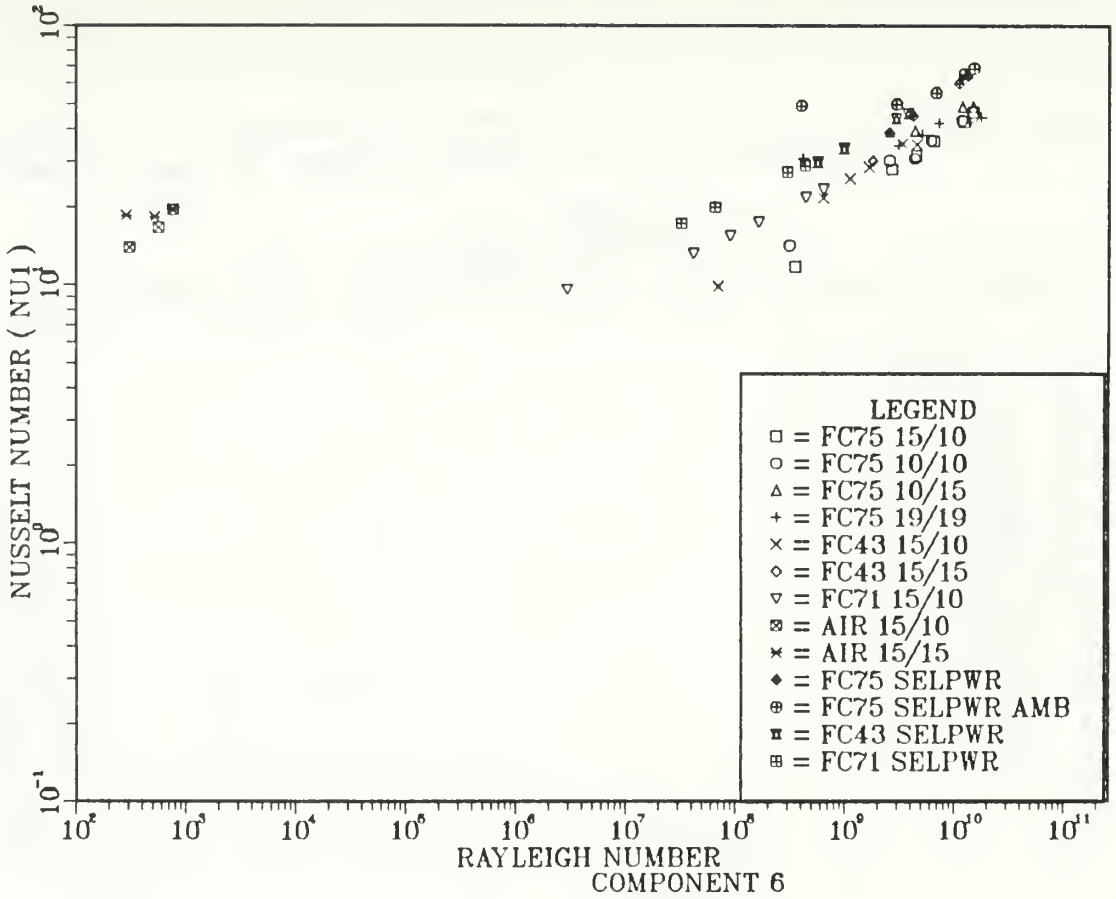

Figure C.6 **Plot of Nusselt Number (Nu1) vs. Rayleigh Number (Ra_f) for All Data Collected for Component 6.**

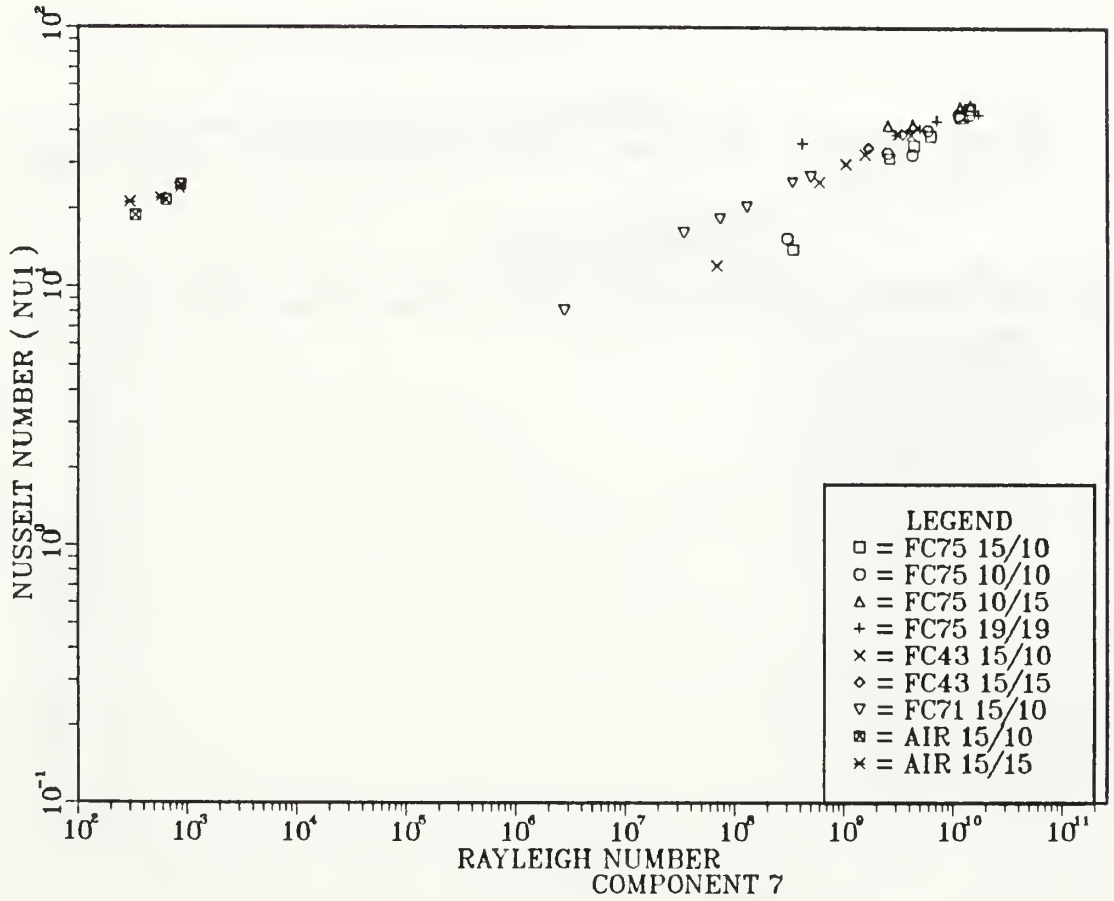

Figure C.7 **Plot of Nusselt Number (Nu1) vs. Rayleigh Number (Ra_f) for All Data Collected for Component 7.**

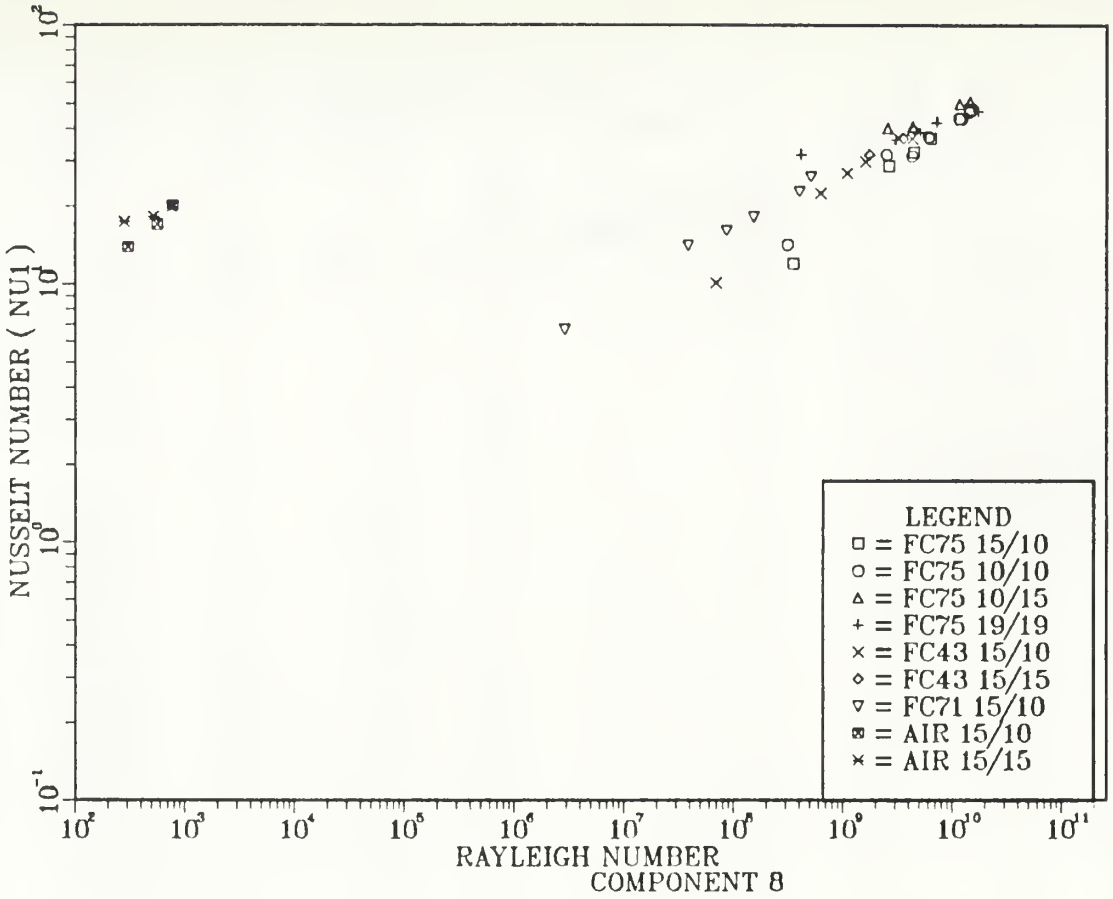

Figure C.8 **Plot of Nusselt Number (Nu1) vs. Rayleigh Number (Ra_f) for All Data Collected for Component 8.**

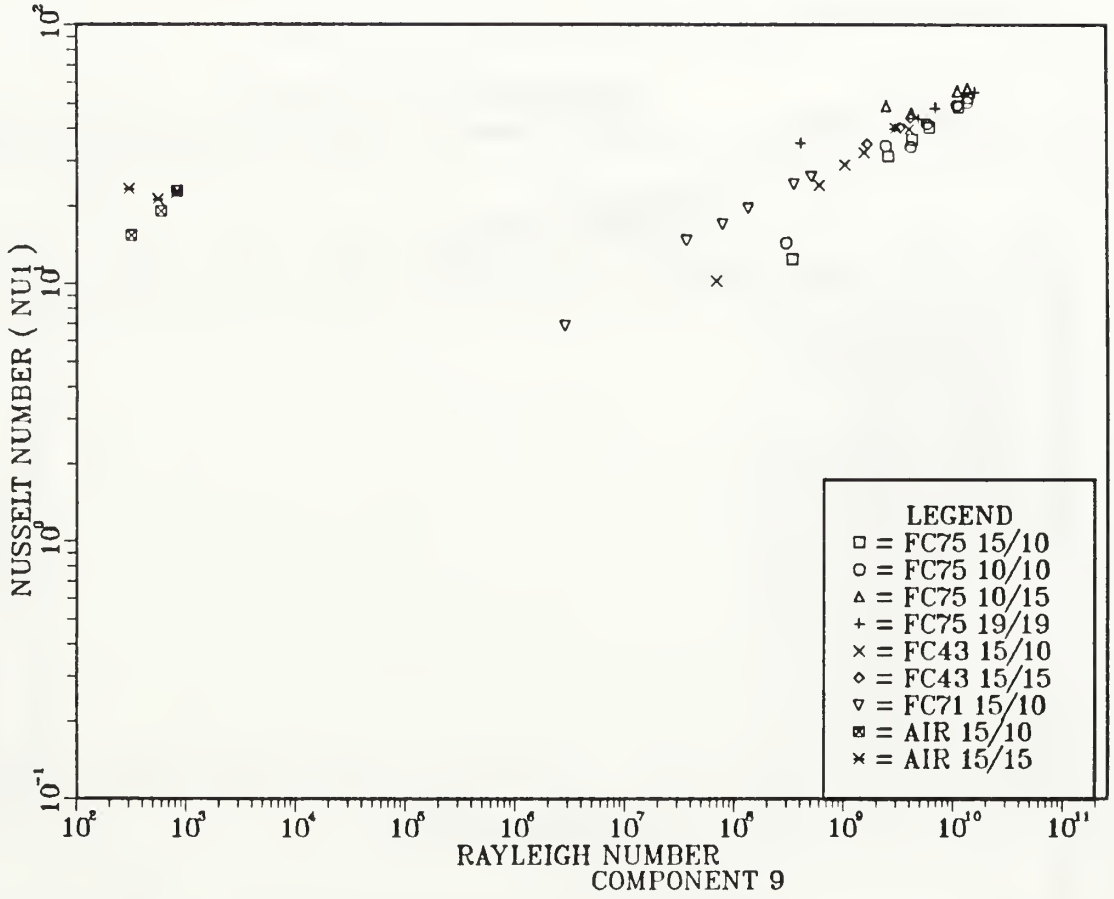

Figure C.9 Plot of Nusselt Number (Nu1) vs. Rayleigh Number (Ra_f) for All Data Collected for Component 9.

LIST OF REFERENCES

1. Oktay, S., " High Heat from Small Package," *Mechanical Engineering* , Vol. 108, pp 36-42, March, 1986.

2. Chu, R., "Heat Transfer in Electronic Systems," *Proc. of the 8 th International Heat Transfer Conference,* San Francisco, California, pp 293-305, 1986.

3. Incropera, F., " Convection Heat Transfer in Electronic Equipment Cooling," *Journal of Heat Transfer*, Vol. 110, pp 1097-1111, November, 1988.

4. Hannemann, R., Incropera, F.P., Simons, R., " Research Needs in Electronic Cooling ," *Proc. of a National Science Foundation / Purdue University Workshop*, Edited by F.P. Incropera, December, 1986.

5. Baker, E., " Liquid Cooling of Microelectronic Devices by Free and Forced Convection ," *Microelectronics and Reliability*, Vol. 11, pp 213-222, April, 1973.

6. Baker, E., "Liquid Immersion Cooling of Small Electronic Devices," *Microelectronics and Reliability* , Vol. 12, pp 163-173, 1973.

7. Park, K.A. and Bergles, A.E., " Natural Convection Heat Transfer Characteristics of Simulated Microelectronic Chips," *Transactions of ASME , Journal of Heat Transfer* , Vol. 109, pp 90-96, February, 1987.

8. Keyhani, M., Prasad, V., and Cox, R., " An Experimental Study of Natural Convection in a Vertical Cavity with Discrete Heat Sources," *ASME* Paper No. 87-HT-76, 1987.

9. Chen, I., Keyhani, M., and Pitts, D.R., " An Experimental Study of Natural Convection Heat Transfer in a Rectangular Enclosure with Protruding Heaters ," Paper presented at National Heat Transfer Conference, Houston, Texas, 1988.

10. Liu, K.V., Kelleher, M.D., and Yang, K.T., " Three Dimensional Natural Convection Cooling of an Array of Heated Protrusions in an Enclosure Filled with a Dielectric Fluid," *Proc. Int. Symposium on Cooling Techniques for Electronic Equipment* , Honolulu, Hawaii, March, 1987.

11. Kelleher, M.D., Knock, R.H., and Yang, K.T., " Laminar Natural Convection in Rectangular Enclosure Due to a Heated Protrusion on One Vertical Wall - Part I: Experimental Investigation", *Proc. 2nd ASME / JSME Thermal Engineering Joint Conference* , Honolulu, Hawaii, pp 169-177, 1987.

12. Lee, K.V., Kelleher, M.D., and Yang, K.T., " Laminar Natural Convection in a Rectangular Enclosure Due to a Heated Protrusion on One Vertical Wall - Part II: Numerical Simulations ", *Proc. 2 nd ASME / JSME Thermal Engineering Joint Conference* , Honolulu, Hawaii, pp 179-185, 1987.

13. Joshi, Y., Kelleher, M.D., and Benedict, T. J., " Natural Convection Immersion Cooling of an Array of Simulated Electronic Components in an Enclosure Filled with Dielectric Fluid ", *Proc. of the International Symposium on Heat Transfer in Electronic and Microelectronic Equipment* Dubrovnik, Yugoslavia, 1988.

14. Knock, R.H., " Flow Visualization Study of Natural Convection from a Heated Protrusion in a Liquid Enclosure ", Master of Science Thesis, Naval Postgraduate School, Monterey, California, December, 1983.

15. Hazard, S.J., " Single Phase Liquid Immersion Cooling of Discrete Heat Sources on a Vertical Channel ", Master of Science Thesis, Naval Postgraduate School, Monterey, California, December, 1986.

16. Pamuk, T., " Natural Convection Immersion Cooling of an Array of Simulated Components in an Enclosure Filled with Discrete Fluid ", Master of Science Thesis, Naval Postgraduate School, Monterey, California, December, 1987.

17. Benedict, T.J., " An Advanced Study of Natural Convection Immersion Cooling of a 3 X 3 Array of Simulated Components in an Enclosure Filled with Dielectric Liquid ", Master of Science Thesis, Naval Postgraduate School, June, 1988.

18. Torres, E., " Natural Convection Cooling of a 3 by 3 Array of Rectangular Protrusions in an Enclosure Filled with Dielectric Liquid: Effects of Boundary Conditions and Component Orientation, Master of Science Thesis, Naval Postgraduate School, December, 1988.

19. Liu, K.V., Yang, K.T., Wu, Y.W. and Kelleher, M.D., " Local Oscillatory Surface Temperature Responses in Immersion Cooling of a Chip Array by Natural Convection in an Enclosure ", *Proc. of the Symposium on Heat and Mass Transfer in Honor of B . T . Chao* , University of Illinois, Urbana - Champaign, pp 309-330, October, 1987.

INITIAL DISTRIBUTION LIST

		No. Copies
1.	Defense Technical Information Center Cameron Station Alexandria, VA 22304-6145	2
2.	Library, Code 0142 Naval Postgraduate School Monterey CA 93943-5002	2
3.	Professor Y. Joshi, Code 69JI Department of Mechanical Engineering Naval Postgraduate School Monterey CA 93943-5004	2
4.	Professor M.D. Kelleher, Code 69Kk Department of Mechanical Engineering Naval Postgraduate School Monterey CA 93943-5004	1
5.	Department Chairman, Code 69 Department of Mechanical Engineering Naval Postgraduate School Monterey CA 93943-5004	1
6.	Mr. Duane Embree Naval Weapons Support Center Code 6042 Crane, IN 47522	1
7.	Mr. Alan Bosler Naval Weapons Support Center Code 6042 Crane, IN 47522	1
8.	Mr. Joseph Cipriano Executive Director Weapons and Combat Systems Directorate Naval Sea Systems Command Washington D.C. 20362-5101	1

9. Naval Engineering Curricular Officer, Code 34 — 1
Department of Mechanical Engineering
Naval Postgraduate School
Monterey CA 93943-5004

10. Professor H. Julien — 1
Department of Mechanical Engineering
Box 3001 Dept. 3450
New Mexico State University
Las Cruces NM 88003

11. Lt. Mark E. Powell USN — 2
P.O. Box 216
Omena MI 49674

Thesis
P7683
c.1

Powell
Natural convection from an array of rectangular protrusions in an enclosure filled with dielectric fluid.